PAPER

An inverse acoustic-elastic interaction problem with phased or phaseless far-field data

To cite this article: Heping Dong et al 2020 Inverse Problems 36 035014

View the <u>article online</u> for updates and enhancements.



IOP ebooks™

Bringing you innovative digital publishing with leading voices to create your essential collection of books in STEM research.

Start exploring the collection - download the first chapter of every title for free.

An inverse acoustic-elastic interaction problem with phased or phaseless far-field data

Heping Dong¹, Jun Lai² and Peijun Li³

- ¹ School of Mathematics, Jilin University, Changchun, Jilin 130012, People's Republic of China
- ² School of Mathematical Sciences, Zhejiang University, Hangzhou, Zhejiang 310027, People's Republic of China
- ³ Department of Mathematics, Purdue University, West Lafayette, IN 47907, United States of America

E-mail: dhp@jlu.edu.cn, laijun6@zju.edu.cn and lipeijun@math.purdue.edu

Received 10 July 2019, revised 12 December 2019 Accepted for publication 8 January 2020 Published 12 February 2020



Abstract

Consider the scattering of a time-harmonic acoustic plane wave by a bounded elastic obstacle which is immersed in a homogeneous acoustic medium. This paper is concerned with an inverse acoustic-elastic interaction problem, which is to determine the location and shape of the elastic obstacle by using either the phased or phaseless far-field data. By introducing the Helmholtz decomposition, the model problem is reduced to a coupled boundary value problem of the Helmholtz equations. The jump relations are studied for the second derivatives of the single-layer potential in order to deduce the corresponding boundary integral equations. The well-posedness is discussed for the solution of the coupled boundary integral equations. An efficient and high order Nyström-type discretization method is proposed for the integral system. A numerical method of nonlinear integral equations is developed for the inverse problem. For the case of phaseless data, we show that the modulus of the far-field pattern is invariant under a translation of the obstacle. To break the translation invariance, an elastic reference ball technique is introduced. We prove that the inverse problem with phaseless far-field pattern has a unique solution under certain conditions. In addition, a numerical method of the reference ball technique based nonlinear integral equations is proposed for the phaseless inverse problem. Numerical experiments are presented to demonstrate the effectiveness and robustness of the proposed methods.

Keywords: elastic wave equation, inverse fluid-solid interaction problem, phaseless data, Helmholtz decomposition, boundary integral equations

(Some figures may appear in colour only in the online journal)

1. Introduction

Consider the scattering of a time-harmonic acoustic plane wave by a bounded penetrable obstacle, which is immersed in an open space occupied by a homogeneous acoustic medium such as some compressible inviscid air or fluid. The obstacle is assumed to be a homogeneous and isotropic elastic medium. When the incident wave impinges the obstacle, a scattered acoustic wave will be generated in the open space and an elastic wave is induced simultaneously inside the obstacle. This scattering phenomenon leads to an acoustic-elastic interaction problem (AEIP). Given the incident wave and the obstacle, the direct acoustic-elastic interaction problem (DAEIP) is to determine the pressure of the acoustic wave field and the displacement of the elastic wave field in the open space and in the obstacle, respectively; the inverse acoustic-elastic interaction problem (IAEIP) is to determine the elastic obstacle from the far-field pattern of the acoustic wave field. The AEIPs have received ever-increasing attention due to their significant applications in seismology and geophysics [35]. Despite many work done so far for both of the DAEIP and IAEIP, they still present many challenging mathematical and computational problems due to the complex of the model equations and the associated Green tensor, as well as the nonlinearity and ill-posedness.

The phased IAEIP refers to the IAEIP that determines the location and shape of the elastic obstacle from the phased far-field data, which contains both the phase and amplitude information. It has been extensively studied in the recent decades. In [10, 11], an optimization based variational method and a decomposition method were proposed to the IAEIP. The direct imaging methods, such as the linear sampling method [40, 41] and the factorization method [16, 29, 49], were also developed to the corresponding inverse problems with far-field and near-field data. For the theoretical analysis, the uniqueness results may be found in [40, 43] for the phased IAEIP.

In many practical applications, the phase of a signal can not be measured accurately compared with its modulus or intensity. Thus it is often desirable to solve the problems with phaseless data, which are called phase or phase retrieval problems. These problems have a long history in industry. They arise from diverse fields of science and engineering, such as electron microscopy, astronomy, crystallography, optical imaging, and so on. We refer to [44, 46] for a review on various methods of recovering phases for phase retrieval problems in protein crystallography and optical imaging, respectively. It is worthy to point out the method of phase retrieval combining holography [12], which is to interfer an electromagnetic field carrying some image with another electromagnetic field of the same frequency and a known structure. The method developed in this work is indeed closely related to the holography.

The phaseless IAEIP is to determine the location and shape of the elastic obstacle from the modulus of the far-field acoustic scattering data, which contains only the amplitude information. Due to the translation invariance property of the phaseless far-field field, it is impossible to uniquely determine the location of the unknown object by a plane incident wave, which makes the phaseless inverse problem much more challenging than the phased counterpart. Various numerical methods have been proposed to solve the phaseless inverse obstacle scattering problems, especially for the acoustic waves which are governed by the scalar Helmholtz equation. For the shape reconstruction with one incident plane wave, we refer to

the Newton iterative method [33], the nonlinear integral equation method [17, 19], the fundamental solution method [27], and the hybrid method [36]. In particular, the nonlinear integral equation method, which was proposed by Johansson and Sleeman [25], was extended to reconstruct the shape of a sound-soft crack by using phaseless far-field data from a single incident plane wave [13]. To reconstruct the location and shape simultaneously, Zhang et al [54, 55] proposed an iterative method by using the superposition of two plane waves with different incident directions to reconstruct the unknown object. In [22], a phase retrieval technique combined with the direct sampling method was proposed to reconstruct the location and shape of an obstacle from phaseless far-field data. The method was extended to the phaseless inverse elastic scattering problem and phaseless IAEIP [21]. We refer to [45, 47, 50, 52, 53] for the uniqueness results on the inverse scattering problems by using phaseless data. Related phaseless inverse scattering problems as well as numerical methods can be found in [1, 3–5, 23, 30, 37, 51]. Recently, a reference ball technique based nonlinear integral equations method was proposed in [9] to break the translation invariance from phaseless far-field data by one incident plane wave. In our recent work [8], we extended this method to the inverse elastic scattering problem with phaseless far-field data by using a single incident plane wave to recover both the location and shape of a rigid elastic obstacle.

In this paper, we consider both the DAEIP and IAEIP. In particular, we study the IAEIP of determining the location and shape of an elastic obstacle from the phased or phaseless far-field data with a single incident plane wave. The goal of this work is fivefold:

- (1) deduce the jump relations for the second derivatives of the single-layer potential and the coupled system of boundary integral equations;
- (2) prove the well-posedness of the solution for the coupled system and develop a Nyströmtype discretization for the boundary integral equations;
- (3) show the translation invariance of the phaseless far-field pattern and present a uniqueness result for the phaseless IAEIP;
- (4) propose a numerical method of nonlinear integral equations to reconstruct the obstacle's location and shape by using the phased far-field data from a single plane incident wave;
- (5) develop a reference ball based method to reconstruct both the obstacle's location and shape by using phaseless far-field data from a single plane incident wave.

For the direct problem, instead of considering directly the coupled acoustic and elastic wave equations, we make use of the Helmholtz decomposition and reduce the model problem into a coupled boundary value problem of the Helmholtz equations. The method of boundary integral equations is adopted to solve the coupled Helmholtz system. However, the boundary conditions are more complicated, since the second derivatives of surface potentials are involved due to the traction operator. Therefore, we investigate carefully the jump relations for the second derivatives of the single-layer potential and deduce coupled boundary integral equations. Moreover, we prove the existence and uniqueness for the solution of the coupled boundary integral equations, and develop a Nyström-type discretization to efficiently and accurately solve the direct acoustic-elastic interaction problem. The proposed method is extremely efficient for the direct scattering problem since we only need to solve the scalar Helmholtz equations instead of solving the vector Navier equations. Related work on the direct acoustic-elastic interaction problems and time-domain acoustic-elastic interaction problem can be found in [2, 24, 39, 48].

For the inverse problem, motivated by the reference ball technique [38, 50] and the recent work [8, 9], we give a uniqueness result for the phaseless IAEIP by introducing an elastic reference ball, and also propose a nonlinear integral equations based iterative numerical scheme to solve the phased and phaseless IAEIP. Since the location of reference ball is known, the

method breaks the translation invariance and is able to recover the location information of the obstacle with negligible additional computational costs. Numerical results show that the method is effective and robust to reconstruct the obstacle with either the phased or phaseless far-field data.

The paper is organized as follows. In section 2, we introduce the coupled acoustic-elastic interaction problem and show the uniqueness for the coupled boundary value problem by using the Helmholtz decomposition. In section 3, we study the jump properties for the second derivatives of the single-layer potential and deduce the coupled boundary integral equations. The existence and uniqueness are established for the solution of the coupled boundary integral equations. Section 4 is devoted to the translation invariance and the uniqueness for the phaseless IAEIP. Section 5 presents a high order Nyström-type discretization to solve the coupled boundary value problem. In section 6, a method of nonlinear integral equations and a reference ball based method are developed to solve the phased and phaseless inverse problems, respectively. Numerical experiments are presented to demonstrate the effectiveness of the proposed methods in section 7. The paper is concluded with some general remarks and directions for future work in section 8.

2. Problem formulation

Consider the scattering problem of a time-harmonic acoustic plane wave by a two-dimensional (2D) elastic obstacle D with a sufficiently smooth boundary Γ_D . The elastic obstacle D is assumed to be homogeneous and isotropic with a mass density ρ_e , and the exterior domain $\mathbb{R}^2 \setminus \overline{D}$ is assumed to be filled with a homogeneous and compressible inviscid air or fluid with a mass density $\rho_a > 0$. Denote by $\nu = (\nu_1, \nu_2)^{\top}$ and $\tau = (-\nu_2, \nu_1)^{\top}$ the unit normal vector and the tangential vector on Γ_D , respectively. Let $\nu_{\perp} = (\nu_2, -\nu_1)^{\top} = -\tau$. Given a vector function $U = (U_1, U_2)^{\top}$ and a scalar function u, we introduce the scalar and vector curl operators

$$\operatorname{curl} \boldsymbol{U} = \partial_{x_1} U_2 - \partial_{x_2} U_1, \quad \operatorname{\boldsymbol{curl}} \boldsymbol{u} = (\partial_{x_2} \boldsymbol{u}, -\partial_{x_1} \boldsymbol{u})^\top.$$

Specifically, the time-harmonic acoustic plane wave is given by $u^{\text{inc}}(x) = e^{i\kappa_a x \cdot d}$, where $d = (\cos \theta, \sin \theta)^{\top}$ is the propagation direction vector, and $\theta \in [0, 2\pi)$ is the incident angle. Given the incident field u^{inc} , the direct problem is to find the elastic wave displacement $U \in (C^2(D) \cap C^1(\overline{D}))^2$ and the acoustic wave pressure $u \in C^2(\mathbb{R}^2 \setminus \overline{D}) \cap C^1(\mathbb{R}^2 \setminus D)$, which satisfy the Navier equation and the Helmholtz equation, respectively:

$$\mu \Delta \mathbf{U} + (\lambda + \mu) \nabla \nabla \cdot \mathbf{U} + \omega^2 \rho_{\rm e} \mathbf{U} = 0 \quad \text{in } D, \tag{2.1}$$

$$\Delta u + \kappa_a^2 u = 0 \quad \text{in } \mathbb{R}^2 \setminus \overline{D}. \tag{2.2}$$

Moreover, U and u are required to satisfy the transmission conditions

$$T(\boldsymbol{U}) = -u\nu, \quad \boldsymbol{U} \cdot \nu = \frac{1}{\omega^2 \rho_a} \partial_{\nu} u \quad \text{on } \Gamma_D.$$
 (2.3)

The scattered acoustic wave pressure $u^s := u - u^{inc}$ is required to satisfy the Sommerfeld radiation condition

$$\lim_{r \to \infty} r^{\frac{1}{2}} (\partial_r u^s - i\kappa_a u^s) = 0, \quad r = |x|.$$

$$(2.4)$$

Here $\omega > 0$ is the angular frequency, $\kappa_{\rm a} = \omega/c$ is the wavenumber in the air/fluid with the sound speed c, and λ , μ are the Lamé parameters satisfying $\mu > 0$, $\lambda + \mu > 0$. The traction operator T is defined by

$$T(\mathbf{U}) := \mu \partial_{\nu} \mathbf{U} + (\lambda + \mu)(\nabla \cdot \mathbf{U})\nu.$$

It has been shown (see [39, 48]) that with a slightly different definition of traction operator T, the scattering problem (2.1)–(2.4) admits a unique solution (U, u) for all but some particular frequencies ω , which are called the Jones frequencies [26]. At the Jones frequency, the acoustic wave field u is unique, but the elastic field U is not unique. In our case, although the definition of the traction operator is different, following exactly the same argument as that in [39, 48], we can also show the existence of the solution (U, u) for all ω except the Jones frequencies. Since the Jones frequency happens only for some special geometries [26], for simplicity, we assume that D does not admit any Jones mode and the AEIP (2.1)–(2.4) has a unique solution (U, u) throughout this work.

For any solution U of the elastic wave equation (2.1), we introduce the Helmholtz decomposition

$$U = \nabla \phi + \operatorname{curl} \psi, \tag{2.5}$$

where ϕ , ψ are two scalar potential functions. Substituting (2.5) into (2.1) yields

$$\nabla[(\lambda + 2\mu)\Delta\phi + \omega^2\rho_e\phi] + \mathbf{curl}\,(\mu\Delta\psi + \omega^2\rho_e\psi) = 0,$$

which is fulfilled if ϕ and ψ satisfies the Helmholtz equation with a different wavenumber

$$\Delta \phi + \kappa_{\rm p}^2 \phi = 0, \quad \Delta \psi + \kappa_{\rm s}^2 \psi = 0.$$

Here

$$\kappa_{\rm p} = \omega \left(\frac{\rho_{\rm e}}{\lambda + 2\mu}\right)^{1/2}, \quad \kappa_{\rm s} = \omega \left(\frac{\rho_{\rm e}}{\mu}\right)^{1/2},$$

is the compressional wavenumber and the shear wavenumber, respectively.

Substituting the Helmholtz decomposition into (2.3) and taking the dot product with ν and τ , respectively, we obtain

$$\mu\nu \cdot \partial_{\nu}\nabla\phi + \mu\nu \cdot \partial_{\nu}\mathbf{curl}\,\psi - (\lambda + \mu)\kappa_{p}^{2}\phi + u^{s} = f_{1},$$

$$\mu\tau \cdot \partial_{\nu}\nabla\phi + \mu\tau \cdot \partial_{\nu}\mathbf{curl}\,\psi = f_{2},$$

$$\partial_{\nu}\phi + \partial_{\tau}\psi - \partial_{\nu}u^{s}/(\omega^{2}\rho_{a}) = f_{3},$$

where

$$f_1 = -u^{\text{inc}}, \quad f_2 = 0, \quad f_3 = \partial_{\nu} u^{\text{inc}} / (\omega^2 \rho_a).$$

In summary, the scalar potential functions ϕ , ψ and the scattered acoustic wave u^s satisfy the following coupled boundary value problem

coupled boundary value problem
$$\begin{cases} \Delta \phi + \kappa_{\rm p}^2 \phi = 0, & \Delta \psi + \kappa_{\rm s}^2 \psi = 0, & \text{in } D, \\ \Delta u^{\rm s} + \kappa_{\rm a}^2 u^{\rm s} = 0, & \text{in } \mathbb{R}^2 \setminus \overline{D}, \\ \mu \nu \cdot \partial_{\nu} \nabla \phi + \mu \nu \cdot \partial_{\nu} \mathbf{curl} \psi - (\lambda + \mu) \kappa_{\rm p}^2 \phi + u^{\rm s} = f_1, & \text{on } \Gamma_D, \\ \tau \cdot \partial_{\nu} \nabla \phi + \tau \cdot \partial_{\nu} \mathbf{curl} \psi = f_2, & \text{on } \Gamma_D, \\ \partial_{\nu} \phi + \partial_{\tau} \psi - \partial_{\nu} u^{\rm s} / (\omega^2 \rho_{\rm a}) = f_3, & \text{on } \Gamma_D, \\ \lim_{r \to \infty} r^{\frac{1}{2}} (\partial_r u^{\rm s} - \mathrm{i} \kappa_{\rm a} u^{\rm s}) = 0, & r = |x|. \end{cases}$$
(2.6)

The following result concerns the uniqueness of the boundary value problem (2.6).

Theorem 2.1. The coupled boundary value problem (2.6) has at most one solution for $\kappa_p > 0$, $\kappa_s > 0$, $\kappa_a > 0$.

Proof. It suffices to show that $\phi = \psi = u^s = 0$ when $f_1 = f_2 = f_3 = 0$. It follows from straightforward calculations that

$$\begin{split} &-\int_{\Gamma_D} u^s \overline{\partial_\nu u^s} \mathrm{d} s = \omega^2 \rho_\mathrm{a} \int_{\Gamma_D} (\mu \nu \cdot \partial_\nu \nabla \phi + \mu \nu \cdot \partial_\nu \mathbf{curl} \ \psi - (\lambda + \mu) \kappa_\mathrm{p}^2 \phi) (\partial_\nu \overline{\phi} + \partial_\tau \overline{\psi}) \mathrm{d} s \\ &= \omega^2 \rho_\mathrm{a} \int_{\Gamma_D} (\mu \partial_\nu (\nabla \phi + \mathbf{curl} \ \psi) \cdot \nu - (\lambda + \mu) \kappa_\mathrm{p}^2 \phi) \left((\nabla \overline{\phi} + \mathbf{curl} \ \overline{\psi}) \cdot \nu \right) \mathrm{d} s \\ &+ \omega^2 \rho_\mathrm{a} \int_{\Gamma_D} (\mu \partial_\nu (\nabla \phi + \mathbf{curl} \ \psi) \cdot \tau) \left((\nabla \overline{\phi} + \mathbf{curl} \ \overline{\psi}) \cdot \tau \right) \mathrm{d} s \\ &= \omega^2 \rho_\mathrm{a} \int_{\Gamma_D} \left(\mu \partial_\nu (\nabla \phi + \mathbf{curl} \ \psi) \cdot \nu \nu + \mu \partial_\nu (\nabla \phi + \mathbf{curl} \ \psi) \cdot \tau \tau - (\lambda + \mu) \kappa_\mathrm{p}^2 \phi \nu \right) \\ &\cdot \left((\nabla \overline{\phi} + \mathbf{curl} \ \overline{\psi}) \cdot \nu \nu + (\nabla \overline{\phi} + \mathbf{curl} \ \overline{\psi}) \cdot \tau \tau \right) \mathrm{d} s \\ &= \omega^2 \rho_\mathrm{a} \int_{\Gamma_D} \left(\mu \partial_\nu (\nabla \phi + \mathbf{curl} \ \psi) - (\lambda + \mu) \kappa_\mathrm{p}^2 \phi \nu \right) \cdot (\nabla \overline{\phi} + \mathbf{curl} \ \overline{\psi}) \mathrm{d} s \\ &= \omega^2 \rho_\mathrm{a} \int_D (\mu \nabla (\nabla \phi + \mathbf{curl} \ \psi) : \nabla (\nabla \overline{\phi} + \mathbf{curl} \ \overline{\psi}) + (\lambda + \mu) \nabla \cdot (\nabla \phi + \mathbf{curl} \ \psi) \\ \nabla \cdot (\nabla \overline{\phi} + \mathbf{curl} \ \overline{\psi}) - \omega^2 \rho_\mathrm{e} (\nabla \phi + \mathbf{curl} \ \psi) \cdot (\nabla \overline{\phi} + \mathbf{curl} \ \overline{\psi}) \mathrm{d} s = 0, \end{split}$$

where $A: B = \operatorname{tr}(AB^{\top})$ is the Frobenius inner product of square matrices A and B. The last two identities follow from Green's formula and the Navier equation (2.1). Taking the imaginary part of the above equation yields

$$\Im \int_{\Gamma_D} u^s \overline{\partial_\nu u^s} \mathrm{d}s = 0,$$

which gives that $u^s = 0$ in $\mathbb{R}^2 \setminus \overline{D}$ by Rellich's lemma. Using the continuity conditions (2.3), we conclude that U is identically zero in D provided that there is no Jones mode in D. Hence,

$$\nabla \phi = -\mathbf{curl} \ \psi \quad \text{in } D,$$

which implies $\Delta \phi = 0$ and $\Delta \psi = 0$. The proof is completed by noting that $\Delta \phi = -\kappa_{\rm p}^2 \phi = 0$ and $\Delta \psi = -\kappa_{\rm s}^2 \psi = 0$ in D.

It is known that a radiating solution of the Helmholtz equation (2.2) has the asymptotic behaviour of the form

$$u^{s}(x) = \frac{e^{i\kappa_{a}|x|}}{\sqrt{|x|}} \left\{ u_{\infty}(\hat{x}) + \mathcal{O}\left(\frac{1}{|x|}\right) \right\} \quad \text{as } |x| \to \infty,$$

uniformly in all directions $\hat{x} := x/|x|$. The function u_{∞} , defined on the unit circle $\Omega = \{x \in \mathbb{R}^2 : |x| = 1\}$, is known as the far-field pattern of u^s . Let $B = \{x \in \mathbb{R}^2 : |x - x_0| < R\}$ be an artificially added elastic ball centered at x_0 such that $B \subset \mathbb{R}^2 \setminus \overline{D}$. The problem geometry is shown in figure 1. For brevity, we denote the boundary of D and B by Γ_D and Γ_B , respectively. The phased and phaseless IAEIP can be stated as follows:

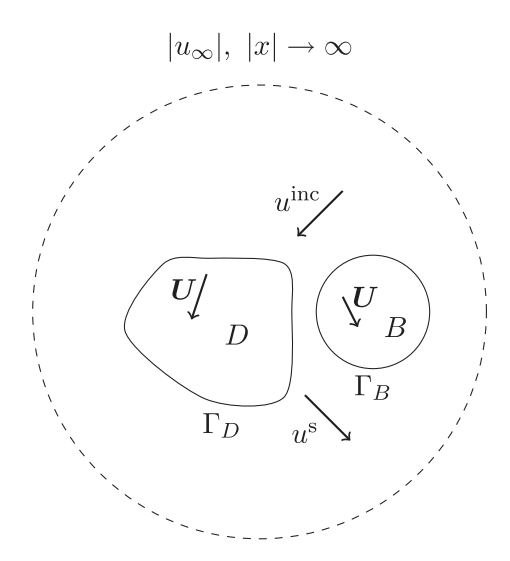


Figure 1. Geometry of the scattering problem with a reference ball.

Problem 1 (Phased IAEIP). Given an incident plane wave u^{inc} with a single incident direction d and the corresponding far-field pattern $u_{\infty}(\hat{x})$, $\forall \hat{x} \in \Omega$ due to the unknown obstacle D, the inverse problem is to determine the location and shape of the boundary Γ_D .

Problem 2 (Phaseless IAEIP). Given an incident plane wave u^{inc} with a single incident direction d and the corresponding phaseless far-field pattern $|u_{\infty}(\hat{x})|$, $\forall \hat{x} \in \Omega$ due to the scatterer $D \cup B$, the inverse problem is to determine the location and shape of the boundary Γ_D .

3. Boundary integral equations

In this section, we derive the boundary integral equations for the coupled boundary value problem (2.6) and discuss their well-posedness.

3.1. Jump relations

We begin with investigating the jump relations for the surface potentials at the boundary Γ_D . For given vectors $a = (a_1, a_2)^{\top} \in \mathbb{R}^2$, denote

$$\nabla a = (\nabla a_1, \nabla a_2)^{\top}, \quad \nabla a^{\top} = (\nabla a_1, \nabla a_2) = (\nabla a_1)^{\top}.$$

For a given scalar function f(x, y), define

$$\mathbf{\nabla}_{\mathbf{y}}(\nabla_{\mathbf{x}}f) = \nabla_{\mathbf{x}}\nabla_{\mathbf{y}}^{\top}f = \begin{bmatrix} \partial_{x_{1}y_{1}}^{2}f & \partial_{x_{1}y_{2}}^{2}f \\ \partial_{x_{2}y_{1}}^{2}f & \partial_{x_{2}y_{2}}^{2}f \end{bmatrix}$$

and

$$(\nabla_{\boldsymbol{x}}\nabla_{\boldsymbol{y}}^{\top}f,\boldsymbol{\nu}) = \begin{bmatrix} \partial_{\boldsymbol{x}_{1}\boldsymbol{y}_{1}}^{2}f & \partial_{\boldsymbol{x}_{1}\boldsymbol{y}_{2}}^{2}f \\ \partial_{\boldsymbol{x}_{2}\boldsymbol{y}_{1}}^{2}f & \partial_{\boldsymbol{x}_{2}\boldsymbol{y}_{2}}^{2}f \end{bmatrix} \begin{bmatrix} \boldsymbol{\nu}_{1} \\ \boldsymbol{\nu}_{2} \end{bmatrix}, \quad (\mathbf{curl}_{\boldsymbol{x}}\nabla_{\boldsymbol{y}}^{\top}f,\boldsymbol{\nu}) = \begin{bmatrix} \partial_{\boldsymbol{x}_{2}\boldsymbol{y}_{1}}^{2}f & \partial_{\boldsymbol{x}_{2}\boldsymbol{y}_{2}}^{2}f \\ -\partial_{\boldsymbol{x}_{1}\boldsymbol{y}_{1}}^{2}f & -\partial_{\boldsymbol{x}_{1}\boldsymbol{y}_{2}}^{2}f \end{bmatrix} \begin{bmatrix} \boldsymbol{\nu}_{1} \\ \boldsymbol{\nu}_{2} \end{bmatrix}.$$

Denote the fundamental solution of the 2D Helmholtz equation by

$$\Phi(x, y; \kappa) = \frac{\mathrm{i}}{4} H_0^{(1)}(\kappa |x - y|), \quad x \neq y,$$

where $H_0^{(1)}$ is the Hankel function of the first kind of order zero. The single- and double-layer potentials with density g are defined by

$$\eta(x) = \int_{\Gamma_D} \Phi(x,y;\kappa) g(y) \mathrm{d} s(y), \quad \chi(x) = \int_{\Gamma_D} \frac{\partial \Phi(x,y;\kappa)}{\partial \nu(y)} g(y) \mathrm{d} s(y), \quad x \in \mathbb{R}^2 \setminus \Gamma_D.$$

In addition, we define the tangential-layer potential by

$$\zeta(x) = \int_{\Gamma_D} \frac{\partial \Phi(x, y; \kappa)}{\partial \tau(y)} g(y) \mathrm{d}s(y), \quad x \in \mathbb{R}^2 \setminus \Gamma_D.$$

The jump relations can be found in [6] for the single- and double-layer potentials as $x \to \Gamma_D$. It is necessary to study the jump properties for the derivatives of those layer potentials in order to derive the boundary integral equations for the coupled boundary value problem (2.6).

Lemma 3.1. The first derivatives of the single-layer potential η with density $g \in C^{0,\alpha}(\Gamma_D)$, $0 < \alpha < 1$, can be uniformly extended in a Hölder continuous fashion from $\mathbb{R}^2 \setminus \overline{D}$ into $\mathbb{R}^2 \setminus D$ and from D into \overline{D} with the limiting values

$$(\nabla \eta)_{\pm}(x) = \int_{\Gamma_D} \nabla_x \Phi(x, y; \kappa) g(y) ds(y) \mp \frac{1}{2} \nu(x) g(x), \quad x \in \Gamma_D,$$
 (3.1)

where

$$(\nabla \eta)_{\pm}(x) := \lim_{h \to 0^+} (\nabla \eta)(x \pm h\nu(x)).$$

Moreover, for the single-layer potential η with density $g \in C^{0,\alpha}(\Gamma_D)$, $0 < \alpha < 1$, we have

$$(\mathbf{curl}\ \eta)_{\pm}(x) = \int_{\Gamma_D} \mathbf{curl}_x \Phi(x, y; \kappa) g(y) \mathrm{d}s(y) \pm \frac{1}{2} \tau(x) g(x), \quad x \in \Gamma_D. \tag{3.2}$$

Proof. Noting

$$\nabla_{x}\Phi(x,y;\kappa) = -\nabla_{y}\Phi(x,y;\kappa) \tag{3.3}$$

and

$$\nabla_{y}\Phi(x,y;\kappa) = \nu(y)\frac{\partial\Phi(x,y;\kappa)}{\partial\nu(y)} + \tau(y)\frac{\partial\Phi(x,y;\kappa)}{\partial\tau(y)},$$
(3.4)

we may similarly show (3.1) by following the proof of theorem 2.17 in [6]. It is clear to note (3.2) by combining the fact that **curl** $\eta = (\nabla \eta)_{\perp}$, $\nu_{\perp} = -\tau$ and the jump relation (3.1).

Lemma 3.2. The first derivatives of the double-layer potential χ with density $g \in C^{1,\alpha}(\Gamma_D)$, $0 < \alpha < 1$, can be uniformly extended in a Hölder continuous fashion from $\mathbb{R}^2 \setminus \overline{D}$ into $\mathbb{R}^2 \setminus D$ and from D into \overline{D} with the limiting values

$$(\nabla \chi)_{\pm}(x) = \kappa^{2} \int_{\Gamma_{D}} \Phi(x, y; \kappa) \nu(y) g(y) ds(y) + \int_{\Gamma_{D}} \mathbf{curl}_{x} \Phi(x, y; \kappa) \frac{\partial g}{\partial \tau}(y) ds(y)$$

$$\pm \frac{1}{2} \tau(x) \frac{\partial g}{\partial \tau}(x), \quad x \in \Gamma_{D}.$$
(3.5)

Proof. Using the jump relation (3.2) and the identities

$$\nabla \nabla \cdot b = \Delta b + \mathbf{curl} \operatorname{curl} b$$

and

$$-\Delta\Phi(x, y; \kappa) = \kappa^2\Phi(x, y; \kappa), \quad x \neq y,$$

we may easily show (3.5) by following the proof of theorem 7.32 in [32] and theorem 2.23 in [6].

Theorem 3.3. For the tangential-layer potential ζ with density $g \in C^{1,\alpha}(\Gamma_D)$, $0 < \alpha < 1$, we have

$$(\nabla \zeta)_{\pm}(x) = -\int_{\Gamma_D} \nabla_x \Phi(x, y; \kappa) \frac{\partial g}{\partial \tau}(y) ds(y) \pm \frac{1}{2} \nu(x) \frac{\partial g}{\partial \tau}(x), \quad x \in \Gamma_D. \quad (3.6)$$

Proof. Using integration by parts, we have

$$\zeta(x) = \int_{\Gamma_D} \frac{\partial \Phi(x, y)}{\partial \tau(y)} g(y) ds(y) = \int_0^{2\pi} \frac{\partial_{\varsigma} (\Phi \circ p)(x, \varsigma)}{G(\varsigma)} (g \circ p)(\varsigma) G(\varsigma) d\varsigma$$

$$= (\Phi \circ p)(x, \varsigma)(g \circ p)(\varsigma) \Big|_{\varsigma=0}^{\varsigma=2\pi} - \int_0^{2\pi} (\Phi \circ p)(x, \varsigma)(g \circ p)'(\varsigma) d\varsigma$$

$$= -\int_{\Gamma_D} \Phi(x, y; \kappa) \frac{\partial g}{\partial \tau}(y) ds(y),$$

for $x \in \mathbb{R}^2 \setminus \Gamma_D$, where we have used $\Gamma_D = \{p(\varsigma) = (p_1(\varsigma), p_2(\varsigma)); \ 0 \leqslant \varsigma < 2\pi\}$ and $G(\varsigma) := |p'(\varsigma)|$ is the Jacobian of the transformation. With the help of jump relation (3.1) of the first derivatives of the single-layer potential in Lemma 3.1, we obtain the jump relation (3.6) immediately.

Theorem 3.4. The second derivatives of the single-layer potential η with density $g \in C^{1,\alpha}(\Gamma_D)$, $0 < \alpha < 1$, can be uniformly extended in a Hölder continuous fashion from $\mathbb{R}^2 \setminus \overline{D}$ into $\mathbb{R}^2 \setminus D$ and from D into \overline{D} with the limiting values

$$(\nabla \nabla^{\top} \eta)_{\pm}(x) = -\kappa^{2} \int_{\Gamma_{D}} \Phi(x, y; \kappa) \left[\nu(y) \nu^{\top}(y) \right] g(y) ds(y) - \int_{\Gamma_{D}} \left[\frac{\partial (g \nu)}{\partial \tau}(y) \mathbf{curl}_{x}^{\top} \Phi(x, y; \kappa) \right] ds(y) + \int_{\Gamma_{D}} \left[\frac{\partial (g \tau)}{\partial \tau}(y) \nabla_{x}^{\top} \Phi(x, y; \kappa) \right] ds(y) \mp \frac{1}{2} \frac{\partial (g \nu)}{\partial \tau}(x) \tau^{\top}(x) \mp \frac{1}{2} \frac{\partial (g \tau)}{\partial \tau}(x) \nu^{\top}(x), \quad x \in \Gamma_{D}$$

$$(3.7)$$

and

$$(\mathbf{curl}\nabla^{\top}\eta)_{\pm}(x) = \kappa^{2} \int_{\Gamma_{D}} \Phi(x, y; \kappa) \left[\tau(y)\nu^{\top}(y)\right] g(y) ds(y) + \int_{\Gamma_{D}} \left[\frac{\partial(g\tau)}{\partial \tau}(y) \mathbf{curl}_{x}^{\top} \Phi(x, y; \kappa)\right] ds(y) + \int_{\Gamma_{D}} \left[\frac{\partial(g\nu)}{\partial \tau}(y)\nabla_{x}^{\top} \Phi(x, y; \kappa)\right] ds(y) \pm \frac{1}{2} \frac{\partial(g\tau)}{\partial \tau}(x)\tau^{\top}(x) \mp \frac{1}{2} \frac{\partial(g\nu)}{\partial \tau}(x)\nu^{\top}(x), \quad x \in \Gamma_{D}.$$
(3.8)

Proof. Using (3.3)–(3.4), we have from taking the second derivatives of the single-layer potential that

$$\begin{split} (\nabla \nabla^\top \eta)(x) &= \int_{\Gamma_D} \boldsymbol{\nabla}_x (\nabla_x \boldsymbol{\Phi}(x,y;\kappa)) g(y) \mathrm{d}s(y) = -\boldsymbol{\nabla}_x \int_{\Gamma_D} \nabla_y \boldsymbol{\Phi}(x,y;\kappa) g(y) \mathrm{d}s(y) \\ &= -\boldsymbol{\nabla}_x \int_{\Gamma_D} \nu(y) \frac{\partial \boldsymbol{\Phi}(x,y;\kappa)}{\partial \nu(y)} g(y) \mathrm{d}s(y) - \boldsymbol{\nabla}_x \int_{\Gamma_D} \tau(y) \frac{\partial \boldsymbol{\Phi}(x,y;\kappa)}{\partial \tau(y)} g(y) \mathrm{d}s(y). \end{split}$$

Combining the above equation and the jump relations (3.5)–(3.6) gives (3.7). Analogously, noting **curl** $\eta = (\nabla \eta)_{\perp}, \nu_{\perp} = -\tau$ and $\tau_{\perp} = \nu$, we have

$$(\mathbf{curl} \nabla^{\top} \eta)(x) = \int_{\Gamma_D} \mathbf{\nabla}_x (\nabla_x \Phi(x, y; \kappa))_{\perp} g(y) \mathrm{d}s(y)$$

$$= \mathbf{\nabla}_x \int_{\Gamma_D} \tau(y) \frac{\partial \Phi(x, y; \kappa)}{\partial \nu(y)} g(y) \mathrm{d}s(y) - \mathbf{\nabla}_x \int_{\Gamma_D} \nu(y) \frac{\partial \Phi(x, y; \kappa)}{\partial \tau(y)} g(y) \mathrm{d}s(y).$$

Applying the jump relation (3.5)–(3.6) again yields (3.8).

In view of $\partial_{\nu}(\nabla \eta) = (\nabla \nabla^{\top} \eta, \nu)$, $\partial_{\nu}(\mathbf{curl} \ \eta) = (\mathbf{curl} \nabla^{\top} \eta, \nu)$ and theorem 3.4, we have the following result.

Corollary 3.5. For the single-layer potential η with density $g \in C^{1,\alpha}(\Gamma_D)$, $0 < \alpha < 1$, we have on Γ_D that

$$\begin{split} \frac{\partial (\nabla \eta)_{\pm}}{\partial \nu}(x) &= -\kappa^2 \int_{\Gamma_D} \Phi(x,y;\kappa) \big[\nu(y) \nu^\top(y) \big] \nu(x) g(y) \mathrm{d}s(y) - \int_{\Gamma_D} \frac{\partial \Phi(x,y;\kappa)}{\partial \tau(x)} \frac{\partial (g\nu)}{\partial \tau}(y) \mathrm{d}s(y) \\ &+ \int_{\Gamma_D} \frac{\partial \Phi(x,y;\kappa)}{\partial \nu(x)} \frac{\partial (g\tau)}{\partial \tau}(y) \mathrm{d}s(y) \mp \frac{1}{2} \frac{\partial (g\tau)}{\partial \tau}(x) \end{split}$$

and

$$\begin{split} \frac{\partial (\mathbf{curl} \; \eta)_{\pm}}{\partial \nu}(x) &= \kappa^2 \int_{\Gamma_D} \Phi(x,y;\kappa) \big[\tau(y) \nu^\top(y) \big] \nu(x) g(y) \mathrm{d}s(y) + \int_{\Gamma_D} \frac{\partial \Phi(x,y;\kappa)}{\partial \tau(x)} \frac{\partial (g\tau)}{\partial \tau}(y) \mathrm{d}s(y) \\ &+ \int_{\Gamma_D} \frac{\partial \Phi(x,y;\kappa)}{\partial \nu(x)} \frac{\partial (g\nu)}{\partial \tau}(y) \mathrm{d}s(y) \mp \frac{1}{2} \frac{\partial (g\nu)}{\partial \tau}(x), \end{split}$$

where

$$\frac{\partial (\nabla \eta)_{\pm}}{\partial \nu}(x) = \lim_{h \to 0^{+}} \frac{\partial (\nabla \eta)(x \pm h\nu(x))}{\partial \nu(x)}.$$

3.2. Boundary integral equations

We introduce the single-layer integral operator and the corresponding far-field integral operator

$$S_{\kappa}[g](x) = 2 \int_{\Gamma_D} \Phi(x, y; \kappa) g(y) ds(y), \quad x \in \Gamma_D,$$

$$S_{\kappa}^{\infty}[g](\hat{x}) = \gamma_{\kappa} \int_{\Gamma_D} e^{-i\kappa \hat{x} \cdot y} g(y) ds(y), \quad \hat{x} \in \Omega,$$

where $\gamma_{\kappa}=\mathrm{e}^{\mathrm{i}\pi/4}/\sqrt{8\kappa\pi}$, the normal derivative integral operator

$$K_{\kappa}[g](x) = 2 \int_{\Gamma_D} \frac{\partial \Phi(x, y; \kappa)}{\partial \nu(x)} g(y) ds(y), \quad x \in \Gamma_D,$$

and the tangential derivative integral operator

$$H_{\kappa}[g](x) = 2 \int_{\Gamma_D} \frac{\partial \Phi(x, y; \kappa)}{\partial \tau(x)} g(y) ds(y), \quad x \in \Gamma_D,$$

which is a singular integral operator and the integral exists in the sense of Cauchy principal value, see [32, chapter 7].

Let the solution of (2.6) be given in the form of single-layer potentials, i.e.

$$\phi(x) = \int_{\Gamma_D} \Phi(x, y; \kappa_p) g_1(y) ds(y), \quad x \in D,$$
(3.9)

$$\psi(x) = \int_{\Gamma_D} \Phi(x, y; \kappa_s) g_2(y) \mathrm{d}s(y), \quad x \in D,$$
(3.10)

$$u^{s}(x) = \int_{\Gamma_{a}} \Phi(x, y; \kappa_{a}) g_{3}(y) ds(y), \quad x \in \mathbb{R}^{2} \setminus \overline{D},$$
(3.11)

where the densities $g_1 \in C^{1,\alpha}(\Gamma_D)$, $g_2 \in C^{1,\alpha}(\Gamma_D)$, and $g_3 \in C^{1,\alpha}(\Gamma_D)$.

Letting $x \in D$ tend to boundary Γ_D in (3.9)–(3.10) and $x \in \mathbb{R}^2 \setminus \overline{D}$ tend to boundary Γ_D in (3.11), using the jump relations of the single-layer potentials, lemmas 3.1 and 3.2, corollary 3.5, and the boundary conditions of (2.6), we obtain on Γ_D that

$$\begin{aligned} 2f_{1}(x) &= -\mu\kappa_{\mathrm{p}}^{2}\nu^{\top}S_{\kappa_{\mathrm{p}}}\left[\nu\nu^{\top}g_{1}\right]\nu + \mu\nu^{\top}K_{\kappa_{\mathrm{p}}}\left[\tau\partial_{\tau}g_{1} + g_{1}\partial_{\tau}\tau\right] - \mu\nu^{\top}H_{\kappa_{\mathrm{p}}}\left[\nu\partial_{\tau}g_{1} + g_{1}\partial_{\tau}\nu\right] \\ &+ \mu\kappa_{\mathrm{s}}^{2}\nu^{\top}S_{\kappa_{\mathrm{s}}}\left[\tau\nu^{\top}g_{2}\right]\nu + \mu\nu^{\top}K_{\kappa_{\mathrm{s}}}\left[\nu\partial_{\tau}g_{2} + g_{2}\partial_{\tau}\nu\right] + \mu\nu^{\top}H_{\kappa_{\mathrm{s}}}\left[\tau\partial_{\tau}g_{2} + g_{2}\partial_{\tau}\tau\right] \\ &- (\lambda + \mu)\kappa_{\mathrm{p}}^{2}S_{\kappa_{\mathrm{p}}}\left[g_{1}\right] + S_{\kappa_{\mathrm{a}}}\left[g_{3}\right] + \mu(\nu \cdot \partial_{\tau}\tau)g_{1} + \mu(\nu \cdot \partial_{\tau}\nu)g_{2} + \mu\partial_{\tau}g_{2}, \\ 2f_{2}(x) &= -\kappa_{\mathrm{p}}^{2}\tau^{\top}S_{\kappa_{\mathrm{p}}}\left[\nu\nu^{\top}g_{1}\right]\nu + \tau^{\top}K_{\kappa_{\mathrm{p}}}\left[\tau\partial_{\tau}g_{1} + g_{1}\partial_{\tau}\tau\right] - \tau^{\top}H_{\kappa_{\mathrm{p}}}\left[\nu\partial_{\tau}g_{1} + g_{1}\partial_{\tau}\nu\right] \\ &+ \kappa_{\mathrm{s}}^{2}\tau^{\top}S_{\kappa_{\mathrm{s}}}\left[\tau\nu^{\top}g_{2}\right]\nu + \tau^{\top}K_{\kappa_{\mathrm{s}}}\left[\nu\partial_{\tau}g_{2} + g_{2}\partial_{\tau}\nu\right] + \tau^{\top}H_{\kappa_{\mathrm{s}}}\left[\tau\partial_{\tau}g_{2} + g_{2}\partial_{\tau}\tau\right] \\ &+ (\tau \cdot \partial_{\tau}\tau)g_{1} + \partial_{\tau}g_{1} + (\tau \cdot \partial_{\tau}\nu)g_{2}, \end{aligned} \tag{3.12}$$

$$2f_{3}(x) &= K_{\kappa_{\mathrm{p}}}\left[g_{1}\right] + H_{\kappa_{\mathrm{s}}}\left[g_{2}\right] - K_{\kappa_{\mathrm{a}}}\left[g_{3}\right]/(\omega^{2}\rho_{a}) + g_{1} + g_{3}/(\omega^{2}\rho_{a}). \end{aligned}$$

The far-field pattern is

$$u_{\infty}(\hat{x}) = \gamma_{\kappa_a} \int_{\Gamma_D} e^{-i\kappa_a \hat{x} \cdot y} g_3(y) ds(y), \quad \hat{x} \in \Omega.$$
 (3.13)

We point out that ν and τ inside of $[\cdot]$ are given with respect to the variable y; otherwise ν and τ are taken with respect to the variable x. For brevity, we shall adopt the same notations in the rest of the paper but they should be clear from the context.

Now we discuss the uniqueness and existence of the solution for the integral equation (3.12).

Theorem 3.6. There exists at most one solution to the boundary integral equation (3.12) if κ_a is not the eigenvalue of the interior Dirichlet problem of the Helmholtz equation in D.

Proof. It suffices to show that $g_1 = g_2 = g_3 = 0$ if $f_1 = f_2 = f_3 = 0$ for equations in (3.12). For $x \in \mathbb{R}^2 \setminus \Gamma_D$, we define single-layer potentials

$$\phi(x) = \int_{\Gamma_D} \Phi(x, y; \kappa_p) g_1(y) ds(y),$$

$$\psi(x) = \int_{\Gamma_D} \Phi(x, y; \kappa_s) g_2(y) ds(y),$$

$$u^s(x) = \int_{\Gamma_D} \Phi(x, y; \kappa_a) g_3(y) ds(y).$$

Let

$$\phi(x) = \begin{cases} \phi_i, & x \in D \\ \phi_e, & x \in \mathbb{R}^2 \backslash \overline{D} \end{cases}, \quad \psi(x) = \begin{cases} \psi_i, & x \in D \\ \psi_e, & x \in \mathbb{R}^2 \backslash \overline{D} \end{cases},$$

and

$$u^{\mathrm{s}}(x) = \begin{cases} u_i^{\mathrm{s}}, & x \in D \\ u_e^{\mathrm{s}}, & x \in \mathbb{R}^2 \backslash \overline{D} \end{cases}.$$

Since ϕ_i , ψ_i and u_e^s satisfy the boundary value problem (2.6), they are identically zero by theorem 2.1. Using the jump condition of single layer potentials, we have on ∂D that

$$\phi_e - \phi_i = 0, \quad \psi_e - \psi_i = 0,$$
 (3.14)

$$\partial_{\nu}\phi_{e} - \partial_{\nu}\phi_{i} = -g_{1}, \quad \partial_{\nu}\psi_{e} - \partial_{\nu}\psi_{i} = -g_{2}. \tag{3.15}$$

Combining (3.14) and the fact $\phi_i = \psi_i = 0$ in D, we derive that ϕ_e and ψ_e satisfy the zero boundary condition on ∂D . By the uniqueness of the exterior problem for the Helmholtz equation, it holds that $\phi_e = \psi_e = 0$ in $\mathbb{R}^2 \setminus \overline{D}$. We conclude that $g_1 = g_2 = 0$ by (3.15). Similarly, we have on ∂D that

$$u_e^{s} - u_i^{s} = 0, (3.16)$$

$$\partial_{\nu}u_{e}^{s} - \partial_{\nu}u_{i}^{s} = -g_{3}. \tag{3.17}$$

By (3.16), we see that u_i^s satisfies the zero Dirichlet boundary condition. Since κ_a is not the eigenvalue of the interior Dirichlet problem, we conclude that u_i^s is identically zero in D, which implies $g_3 = 0$ by (3.17).

Theorem 3.7. There exists a unique solution to the boundary integral equation (3.12) if none of κ_p , κ_s or κ_a is the eigenvalue of the interior Dirichlet problem of the Helmholtz equation in D.

Proof. Since the original coupled equations (2.1)–(2.4) admit a unique solution (u, U), by the Helmholtz decomposition $U = \nabla \phi + \mathbf{curl} \ \psi$, we have on ∂D that

$$\partial_{\nu}\phi + \partial_{\tau}\psi = \boldsymbol{U} \cdot \boldsymbol{\nu}, \quad \partial_{\tau}\psi - \partial_{\nu}\psi = \boldsymbol{U} \cdot \boldsymbol{\tau}.$$

Plugging the single layer representations (3.9) and (3.10) for ϕ and ψ into the above equations and using the jump property of boundary integral operators, we have

$$\begin{cases} (I + K_{\kappa_p})g_1 + H_{\kappa_s}g_2 = 2U \cdot \nu \\ H_{\kappa_p}g_1 - (I + K_{\kappa_s})g_2 = 2U \cdot \tau \end{cases}$$
(3.18)

where I is the identity operator. Following the conclusion in [34, theorem 4.1], we have that the boundary integral equation (3.18) admits a solution (g_1, g_2) when neither κ_p nor κ_s is the eigenvalue of the interior Dirichlet problem of the Helmholtz equation in D. For g_3 , since κ_a is not an interior Dirichlet eigenvalue either, the single layer operator S_{κ_a} is invertible. Therefore

$$g_3 = S_{\kappa_2}^{-1} u^s$$
.

Based on the construction, one can easily see that g_1 , g_2 and g_3 satisfy the boundary integral equation (3.12).

4. Translation invariance and a uniqueness result

In this section, we present the translation invariance of the phaseless far-field pattern and prove a uniqueness result for the phaseless IAEIP. We assume that the solution (U, u^s) solves the following boundary value problem

$$\mu \Delta \mathbf{U} + (\lambda + \mu) \nabla \nabla \cdot \mathbf{U} + \omega^2 \rho_{\rm e} \mathbf{U} = 0 \qquad \text{in } D, \tag{4.1}$$

$$\Delta u^s + \kappa_a^2 u^s = 0 \qquad \qquad \text{in } \mathbb{R}^2 \setminus \overline{D}, \tag{4.2}$$

$$T(\mathbf{U}) + u^s \nu = -u^{\text{inc}} \nu, \quad \partial_{\nu} u^s - \omega^2 \rho_{\text{a}} \mathbf{U} \cdot \nu = -\partial_{\nu} u^{\text{inc}} \quad \text{on } \Gamma_D,$$

$$(4.3)$$

$$\lim_{r \to \infty} r^{\frac{1}{2}} (\partial_r u^s - i\kappa_a u^s) = 0 \tag{4.4}$$

for all ω except the Jones frequencies.

Theorem 4.1. Let u_{∞} be the far field pattern of the scattered waves u^s with the incident plane wave $u^{\text{inc}}(x) = e^{i\kappa_a d \cdot x}$. For the shifted domain $D_h := \{x + h : x \in D\}$ with a fixed vector $h \in \mathbb{R}^2$, the far-field pattern u_{∞}^h satisfies

$$u_{\infty}^{h}(\hat{x}) = e^{i\kappa_{a}(d-\hat{x})\cdot h}u_{\infty}(\hat{x}).$$

Proof. Denote (U_h, u_h^s) by the solution of above boundary value problem (4.1)–(4.4) for D_h . We claim that

$$\begin{cases}
U_h(y) = e^{i\kappa_a d \cdot h} U(y - h), & \forall y \in D_h, \\
u_h^s(y) = e^{i\kappa_a d \cdot h} u^s(y - h), & \forall y \in \mathbb{R}^2 \setminus \overline{D_h}.
\end{cases}$$
(4.5)

In fact, since the boundary value problem (4.1)–(4.4) exists a unique solution and noting that the Sommerfeld radiation condition is invariant under translations of the origin [7], it only need to verify that (U_h, u_h^s) shown in (4.5) satisfies the boundary condition (4.3). That is, $\forall y \in \Gamma_{D_h}$, we have

$$\begin{split} T(\boldsymbol{U_h})(y) + u_h^s(y)\nu_h(y) &= \mathrm{e}^{\mathrm{i}\kappa_a d \cdot h} \bigg(\partial_{\nu_h} \boldsymbol{U}(y-h) + (\lambda + \mu)(\nabla \cdot \boldsymbol{U}(y-h))\nu_h(y) + u^s(y-h)\nu_h(y) \bigg) \\ &= \mathrm{e}^{\mathrm{i}\kappa_a d \cdot h} \bigg(T(\boldsymbol{U})(y-h) + u^s(y-h)\nu(y-h) \bigg) \\ &= \mathrm{e}^{\mathrm{i}\kappa_a d \cdot h} \bigg(- \mathrm{e}^{\mathrm{i}\kappa_a d \cdot (y-h)}\nu(y-h) \bigg) = -u^{\mathrm{inc}}(y)\nu_h(y) \end{split}$$

and the second boundary condition of (4.3) on Γ_{D_h} can be verified in the same way. Using (4.5), we obtain

$$\frac{\partial u_h^s}{\partial \nu_h}(y) = e^{i\kappa_a d \cdot h} \frac{\partial u^s}{\partial \nu}(y - h), \qquad \forall y \in \Gamma_{D_h}. \tag{4.6}$$

Then, combining (4.5) and (4.6) and [7, theorem 2.6], far field pattern satisfies

$$\begin{split} u^h_{\infty}(\hat{x}) &= \gamma_{\kappa_a} \int_{\Gamma_{D_h}} \bigg\{ u^s_h(y) \frac{\partial \mathrm{e}^{-\mathrm{i}\kappa_a \hat{x} \cdot y}}{\partial \nu_h(y)} - \frac{\partial u^s_h}{\partial \nu_h}(y) \mathrm{e}^{-\mathrm{i}\kappa_a \hat{x} \cdot y} \bigg\} \mathrm{d}s(y) \\ &= \mathrm{e}^{\mathrm{i}\kappa_a (d - \hat{x}) \cdot h} \gamma_{\kappa_a} \int_{\Gamma_D} \bigg\{ u^s(y) \frac{\partial \mathrm{e}^{-\mathrm{i}\kappa_a \hat{x} \cdot y}}{\partial \nu(y)} - \frac{\partial u^s}{\partial \nu}(y) \mathrm{e}^{-\mathrm{i}\kappa_a \hat{x} \cdot y} \bigg\} \mathrm{d}s(y) \\ &= \mathrm{e}^{\mathrm{i}\kappa_a (d - \hat{x}) \cdot h} u_{\infty}(\hat{x}) \end{split}$$

which completes the proof.

Theorem 4.1 implies that the location of the obstacle can not be uniquely recovered by the modules of far-field pattern when the plane wave is used as an incident field. To overcome this difficulty, motivated by [50], we may introduce an elastic reference ball $B = B(x_0, R) = \{x \in \mathbb{R}^2 : |x - x_0| < R\}$ to the scattering system in order to break the translation invariance

Assume that P is a disk (with positive radius) such that $P \subset \mathbb{R}^2 \setminus (\overline{D} \cup \overline{B})$ and κ_a^2 is not a Dirichlet eigenvalue of $-\Delta$ in P. Denote the boundary of P by ∂P . Consider that the incident wave is given by a plane wave $u^{\mathrm{inc}}(x,d)$ and a point source $v^{\mathrm{inc}}(x,z)$, i.e. $u^{\mathrm{inc}}(x,d) = \mathrm{e}^{\mathrm{i}\kappa_a x \cdot d}$ and $v^{\mathrm{inc}}(x,z) = \Phi(x,z;\kappa_a)$, where $z \in \partial P$ is the source location. Assume further that $\{u_{D\cup B}^s(x)(x,d), u_{D\cup B}^\infty(\hat{x},z)\}$ and $\{v_{D\cup B}^s(x,z), v_{D\cup B}^\infty(\hat{x},z)\}$ are the scattered field and the farfield pattern generated by $D \cup B$ corresponding to the incident field $u^{\mathrm{inc}}(x,d)$ and $v^{\mathrm{inc}}(x,z)$, respectively.

The next lemma shows a mixed reciprocity relation for the acoustic-elastic interaction problem. A similar result for acoustic obstacle scattering problem can be found in [7, theorem 3.13].

Lemma 4.2 (Mixed reciprocity relation). For acoustic-elastic interaction problem (2.1)–(2.4) with point source v^{inc} and plane wave u^{inc} , we have the relation

$$v^{\infty}(-d,z) = \gamma_{\kappa_a} u^s(z,d), \qquad z \in \mathbb{R}^2 \setminus \bar{D}, \quad d \in \Omega.$$
 (4.7)

Proof. From Green's theorem, we have

$$0 = \int_{\Gamma_D} \left\{ v^{\rm inc}(\cdot, z) \frac{\partial}{\partial \nu} u^{\rm inc}(\cdot, d) - u^{\rm inc}(\cdot, d) \frac{\partial}{\partial \nu} v^{\rm inc}(\cdot, z) \right\} ds$$

$$0 = \int_{\Gamma_D} \left\{ v^s(\cdot, z) \frac{\partial}{\partial \nu} u^s(\cdot, d) - u^s(\cdot, d) \frac{\partial}{\partial \nu} v^s(\cdot, z) \right\} ds.$$

With the aid of [7, theorems 2.5 and 2.6], we have

$$\frac{1}{\gamma_{\kappa_a}}v^{\infty}(-d,z) = \int_{\Gamma_D} \left\{ v^s(\cdot,z) \frac{\partial}{\partial \nu} u^{\mathrm{inc}}(\cdot,d) - u^{\mathrm{inc}}(\cdot,d) \frac{\partial}{\partial \nu} v^s(\cdot,z) \right\} \mathrm{d}s$$

$$u^s(z,d) = \int_{\Gamma_D} \left\{ u^s(\cdot,d) \frac{\partial}{\partial \nu} v^{\mathrm{inc}}(\cdot,z) - v^{\mathrm{inc}}(\cdot,z) \frac{\partial}{\partial \nu} u^s(\cdot,d) \right\} \mathrm{d}s.$$

We now subtract the last equation from the sum of the three preceding equations to obtain

$$\frac{1}{\gamma_{\kappa_a}}v^{\infty}(-d,z)-u^s(z,d)=\int_{\Gamma_D}\left\{v(\cdot,z)\frac{\partial}{\partial\nu}u(\cdot,d)-u(\cdot,d)\frac{\partial}{\partial\nu}v(\cdot,z)\right\}\mathrm{d}s.$$

Using boundary condition (2.3) for solutions (u, U) and (v, V) and the Betti formula, we get

$$\frac{1}{\gamma_{\kappa_a}}v^{\infty}(-d,z)-u^{s}(z,d)=-\omega^2\rho_a\int_{\Gamma_D}\Big\{T(\boldsymbol{V})(\cdot,z)\cdot\boldsymbol{U}(\cdot,d)-T(\boldsymbol{U})(\cdot,d)\cdot\boldsymbol{V}(\cdot,z)\Big\}\mathrm{d}s=0,$$

which gives (4.7) and completes the proof.

Now we present a uniqueness result for the phaseless inverse scattering problem. A similar uniqueness result may be found in [50, theorem 4.1] for the phaseless inverse medium scattering problem.

Theorem 4.3. Let D_1 and D_2 be two elastic obstacles with smooth boundaries, and ω is not a Jones frequency either for D_1 or for D_2 . Suppose that the far-field patterns satisfy the following conditions:

$$|u_{D_1 \cup B}^{\infty}(\hat{x}, d_0)| = |u_{D_2 \cup B}^{\infty}(\hat{x}, d_0)|, \qquad \forall \hat{x} \in \Omega, \tag{4.8}$$

$$|v_{D_1 \cup B}^{\infty}(\hat{x}, z)| = |v_{D_2 \cup B}^{\infty}(\hat{x}, z)|, \qquad \forall (\hat{x}, z) \in \Omega \times \partial P, \tag{4.9}$$

$$|u_{D_1 \cup B}^{\infty}(\hat{x}, d_0) + v_{D_1 \cup B}^{\infty}(\hat{x}, z)| = |u_{D_2 \cup B}^{\infty}(\hat{x}, d_0) + v_{D_2 \cup B}^{\infty}(\hat{x}, z)|, \qquad \forall (\hat{x}, z) \in \Omega \times \partial P$$
(4.10)

for a fixed $d_0 \in \Omega$, then $D_1 = D_2$.

Proof. By (4.8)–(4.10), we have

$$\Re\left\{u_{D_1\cup B}^{\infty}(\hat{x},d_0)\overline{v_{D_1\cup B}^{\infty}(\hat{x},z)}\right\} = \Re\left\{u_{D_2\cup B}^{\infty}(\hat{x},d_0)\overline{v_{D_2\cup B}^{\infty}(\hat{x},z)}\right\}, \quad \forall \hat{x} \in \Omega, z \in \partial P.$$

In view of (4.8) and (4.9), we assume that

$$u^{\infty}_{D_{j}\cup B}(\hat{x},d_{0}) = r(\hat{x},d_{0})e^{\mathrm{i}\alpha_{j}(\hat{x},d_{0})}, \quad v^{\infty}_{D_{j}\cup B}(\hat{x},z) = s(\hat{x},z)e^{\mathrm{i}\beta_{j}(\hat{x},z)}, \quad j=1,2,$$

where $r(\hat{x},d_0)=|u_{D_j\cup B}^{\infty}(\hat{x},d_0)|$, $s(\hat{x},z)=|v_{D_j\cup B}^{\infty}(\hat{x},z)|$, $\alpha_j(\hat{x},d_0)$ and $\beta_j(\hat{x},z)$ are real-valued functions, j=1,2. From Lemma 4.2, we have that

$$v^{\infty}(\hat{x}, z) = \gamma_a u^s(z, -\hat{x}), \quad \forall \hat{x} \in \Omega, z \in \partial P.$$
 (4.11)

Using (4.11) and the analyticity argument in [50, theorem 3.1], we obtain that

$$u_{D_1 \cup B}^{s}(x,d) = e^{i\gamma(-d)} u_{D_2 \cup B}^{s}(x,d), \quad \forall x \in \mathbb{R}^2 \setminus (D_1 \cup D_2 \cup B), \quad -d \in S,$$
(4.12)

where $\gamma(\hat{x}) := \alpha_1(\hat{x}, d_0) - \alpha_2(\hat{x}, d_0) - 2m\pi$, $\hat{x} \in S$, $m \in \mathbb{Z}$, and $S \subset \Omega$ is an open arc. Furthermore, for $x \in \Gamma_B$, $-d \in S$, we get

$$u_{D_1 \cup B}^{s}(x,d) = e^{i\gamma(-d)} u_{D_2 \cup B}^{s}(x,d), \quad \frac{\partial u_{D_1 \cup B}^{s}(x,d)}{\partial \nu} = e^{i\gamma(-d)} \frac{\partial u_{D_2 \cup B}^{s}(x,d)}{\partial \nu}.$$

Noting that the total fields $(u_{D_1 \cup B}, U_{D_1 \cup B})$ and $(u_{D_2 \cup B}, U_{D_2 \cup B})$ are the solutions of (2.1)–(2.4) corresponding to the scatterers $D_1 \cup B$ and $D_2 \cup B$, respectively, we find that

$$\tilde{u}(x,d) := u_{D_1 \cup B}(x,d) - e^{i\gamma(-d)}u_{D_2 \cup B}(x,d), \quad \tilde{U}(x,d) := U_{D_1 \cup B}(x,d) - e^{i\gamma(-d)}U_{D_2 \cup B}(x,d)$$

satisfy the Navier equation and the Helmholtz equation

$$\mu \Delta \widetilde{\boldsymbol{U}} + (\lambda + \mu) \nabla \nabla \cdot \widetilde{\boldsymbol{U}} + \omega^2 \rho_e \widetilde{\boldsymbol{U}} = 0 \quad \text{in } \boldsymbol{B},$$
$$\Delta \widetilde{\boldsymbol{u}} + \kappa_a^2 \widetilde{\boldsymbol{u}} = 0 \quad \text{in } \mathbb{R}^2 \setminus \overline{D_1 \cup D_2 \cup B},$$

and the transmission conditions on Γ_B

$$T(\widetilde{\boldsymbol{U}}) = -\tilde{\boldsymbol{u}}\nu, \quad \widetilde{\boldsymbol{U}} \cdot \nu = \frac{1}{\omega^2 \rho_a} \partial_{\nu} \tilde{\boldsymbol{u}}.$$
 (4.13)

Suppose that $(w(x, d_0), W(x, d_0))$ is the solution of (2.1)–(2.4) corresponding to the single reference ball B with incident plane wave $u^{\text{inc}}(x, d_0)$, then the far-field $w^{\infty}(\hat{x}, d_0) \neq 0$, $\hat{x} \in \Omega$. Using the Betti formula and the transmission condition (4.13), and noting the identity

$$\tilde{u}(x,d) = (1 - e^{i\gamma(-d)})u^{inc}(x,d), \quad \frac{\partial \tilde{u}}{\partial \nu}(x,d) = (1 - e^{i\gamma(-d)})\frac{\partial u^{inc}}{\partial \nu}(x,d), \quad \forall x \in \Gamma_B, -d \in S,$$

we have

$$\begin{split} 0 &= \int_{\Gamma_B} \Big\{ T(\boldsymbol{W})(y,d_0) \cdot \widetilde{\boldsymbol{U}}(y,d) - T(\widetilde{\boldsymbol{U}})(y,d) \cdot \boldsymbol{W}(y,d_0) \Big\} \mathrm{d}s(y) \\ &= \frac{-1}{\omega^2 \rho_\mathrm{a}} \int_{\Gamma_B} \Big\{ w(y,d_0) \frac{\partial \widetilde{\boldsymbol{u}}(y,d)}{\partial \nu} - \widetilde{\boldsymbol{u}}(y,d) \frac{\partial w(y,d_0)}{\partial \nu} \Big\} \mathrm{d}s(y) \\ &= \frac{-(1-\mathrm{e}^{\mathrm{i}\gamma(-d)})}{\omega^2 \rho_\mathrm{a}} \int_{\Gamma_B} \Big\{ w(y,d_0) \frac{\partial u^{\mathrm{inc}}(y,d)}{\partial \nu} - u^{\mathrm{inc}}(y,d) \frac{\partial w(y,d_0)}{\partial \nu} \Big\} \mathrm{d}s(y) \\ &= \frac{-(1-\mathrm{e}^{\mathrm{i}\gamma(-d)})}{\omega^2 \rho_\mathrm{a}} w^\infty (-d,d_0), \quad \forall -d \in S. \end{split}$$

We claim $|w^{\infty}(-d,d_0)| \not\equiv 0, \ \forall -d \in S$. Otherwise, we obtain by using the analytic continuation that $w^{\infty}(\hat{x},d_0)=0, \ \forall \hat{x} \in \Omega$. This is a contradiction. By continuity, there exists an open curve $\tilde{S} \subset S$, such that $|w^{\infty}(-d,d_0)| \neq 0, \ \forall -d \in \tilde{S}$, which implies that $e^{i\gamma(-d)}=1$ for $-d \in \tilde{S}$. From (4.12), we have

$$u_{D_1\cup B}^{\infty}(\hat{x},d) = u_{D_2\cup B}^{\infty}(\hat{x},d), \quad \forall (\hat{x},-d) \in \Omega \times \tilde{S}.$$

Again, using the reciprocity relation and the analyticity of $u_{D_j \cup B}^{\infty}(\hat{x}, d)$ for j = 1, 2, we obtain that the far-field patterns $u_{D_1 \cup B}^{\infty}$ and $u_{D_2 \cup B}^{\infty}$ coincide for all observation and incident directions $\hat{x}, d \in \Omega$. We conclude from [40, theorem 4.1] that $D_1 = D_2$.

Remark 4.4. In view of the proof of theorem 4.3, we can also assume that the scatterers D_1, D_2 and the reference ball *B* possess different mass densities and Lamé parameters.

Remark 4.5. Theorem 4.3 only gives a sufficient condition to uniquely reconstruct the the unknown obstacle D with phaseless data. We expect that the uniqueness result may also hold with much less data. In particular, in our numerical experiments, we do not use the phaseless far-field data generated by the point source $v^{\text{inc}}(x,z)$ with $z \in \partial P$, although in this case, the uniqueness result is still under investigation.

5. Nyström-type discretization for boundary integral equations

In this section, we introduce a Nyström-type discretization for the boundary integral equations and present some effective numerical quadratures to handle the singular integrals.

5.1. Parametrization

For simplicity, the boundary Γ_D is assumed to be an analytic starlike curve with the parametrized form

$$\Gamma_D = \{ p(\hat{x}) = c + r(\hat{x})\hat{x}; \ c = (c_1, c_2)^\top, \ \hat{x} \in \Omega \},$$

where $\Omega = \{\hat{x}(t) = (\cos t, \sin t)^{\top}; \ 0 \le t < 2\pi\}$. We introduce the parametrized integral operators which are still represented by $S_{\kappa}, S_{\kappa}^{\infty}, K_{\kappa}$ and H_{κ} for convenience, i.e.

$$\begin{split} & \left(S_{\kappa}[\vartheta;p]\right)(t) = \int_{0}^{2\pi} \widetilde{M}(t,\varsigma;\kappa)\vartheta(\varsigma)\mathrm{d}\varsigma, \\ & \left(S_{\kappa}^{\infty}[\vartheta;p]\right)(t) = \gamma_{\kappa} \int_{0}^{2\pi} \mathrm{e}^{-\mathrm{i}\kappa\hat{x}(t)\cdot p(\varsigma)}\vartheta(\varsigma)\mathrm{d}\varsigma, \\ & \left(K_{\kappa}[\vartheta;p]\right)(t) = \frac{1}{G(t)} \int_{0}^{2\pi} \widetilde{K}(t,\varsigma;\kappa)\vartheta(\varsigma)\mathrm{d}\varsigma, \\ & \left(H_{\kappa}[\vartheta;p]\right)(t) = \frac{1}{G(t)} \int_{0}^{2\pi} \widetilde{H}(t,\varsigma;\kappa)\vartheta(\varsigma)\mathrm{d}\varsigma, \end{split}$$

where $\vartheta(\varsigma) = G(\varsigma)g(p(\varsigma))$, $G(\varsigma) := |p'(\varsigma)| = \sqrt{(r'(\varsigma))^2 + r^2(\varsigma)}$ is the Jacobian of the transformation,

$$\begin{split} \widetilde{M}(t,\varsigma;\kappa) &= \frac{\mathrm{i}}{2} H_0^{(1)}(\kappa|p(t)-p(\varsigma)|), \\ \widetilde{K}(t,\varsigma;\kappa) &= \frac{\mathrm{i}\kappa}{2} \mathsf{n}(t) \cdot \big[p(\varsigma)-p(t)\big] \frac{H_1^{(1)}(\kappa|p(t)-p(\varsigma)|)}{|p(t)-p(\varsigma)|}, \\ \widetilde{H}(t,\varsigma;\kappa) &= \frac{\mathrm{i}\kappa}{2} \mathsf{n}(t)^\perp \cdot \big[p(\varsigma)-p(t)\big] \frac{H_1^{(1)}(\kappa|p(t)-p(\varsigma)|)}{|p(t)-p(\varsigma)|}, \end{split}$$

and

$$\begin{split} \mathbf{n}(t) &:= \tilde{\nu}(t)|p'(t)| = \left(p_2'(t), -p_1'(t)\right)^\top, \quad \tilde{\nu} = \nu \circ p, \\ \mathbf{n}(t)^\perp &:= \tilde{\tau}(t)|p'(t)| = \left(p_1'(t), p_2'(t)\right)^\top, \quad \tilde{\tau} = \tau \circ p. \end{split}$$

Thus, (3.12) can be reformulated as the parametrized integral equations

$$\begin{split} w_{1} &= -\mu\kappa_{p}^{2}\tilde{\nu}^{\top}S_{\kappa_{p}}\big[\tilde{\nu}\tilde{\nu}^{\top}\varphi_{1}G;p\big]\tilde{\nu} + \mu\tilde{\nu}^{\top}K_{\kappa_{p}}\big[\tilde{\tau}\varphi_{1}' + \tilde{\tau}'\varphi_{1};p\big] - \mu\tilde{\nu}^{\top}H_{\kappa_{p}}\big[\tilde{\nu}\varphi_{1}' + \tilde{\nu}'\varphi_{1};p\big] \\ &+ \mu\kappa_{s}^{2}\tilde{\nu}^{\top}S_{\kappa_{s}}\big[\tilde{\tau}\tilde{\nu}^{\top}\varphi_{2}G;p\big]\tilde{\nu} + \mu\tilde{\nu}^{\top}K_{\kappa_{s}}\big[\tilde{\nu}\varphi_{2}' + \tilde{\nu}'\varphi_{2};p\big] + \mu\tilde{\nu}^{\top}H_{\kappa_{s}}\big[\tilde{\tau}\varphi_{2}' + \tilde{\tau}'\varphi_{2};p\big] \\ &- (\lambda + \mu)\kappa_{p}^{2}S_{\kappa_{p}}[\varphi_{1}G;p] + S_{\kappa_{a}}[\varphi_{3}G;p] + \mu(\tilde{\nu} \cdot \tilde{\tau}')\varphi_{1}/G + \mu(\tilde{\nu} \cdot \tilde{\nu}')\varphi_{2}/G + \mu\varphi_{2}'/G, \\ w_{2} &= -\kappa_{p}^{2}\tilde{\tau}^{\top}S_{\kappa_{p}}\big[\tilde{\nu}\tilde{\nu}^{\top}\varphi_{1}G;p\big]\tilde{\nu} + \tilde{\tau}^{\top}K_{\kappa_{p}}\big[\tilde{\tau}\varphi_{1}' + \tilde{\tau}'\varphi_{1};p\big] - \tilde{\tau}^{\top}H_{\kappa_{p}}\big[\tilde{\nu}\varphi_{1}' + \tilde{\nu}'\varphi_{1};p\big] \\ &+ \kappa_{s}^{2}\tilde{\tau}^{\top}S_{\kappa_{s}}\big[\tilde{\tau}\tilde{\nu}^{\top}\varphi_{2}G;p\big]\tilde{\nu} + \tilde{\tau}^{\top}K_{\kappa_{s}}\big[\tilde{\nu}\varphi_{2}' + \tilde{\nu}'\varphi_{2};p\big] + \tilde{\tau}^{\top}H_{\kappa_{s}}\big[\tilde{\tau}\varphi_{2}' + \tilde{\tau}'\varphi_{2};p\big] \\ &+ (\tilde{\tau} \cdot \tilde{\tau}')\varphi_{1}/G + \varphi_{1}'/G + (\tilde{\tau} \cdot \tilde{\nu}')\varphi_{2}/G, \\ w_{3} &= K_{\kappa_{p}}\big[\varphi_{1}G;p\big] + H_{\kappa_{s}}\big[\varphi_{2}G;p\big] - K_{\kappa_{a}}\big[\varphi_{3}G;p\big]/(\omega^{2}\rho_{a}) + \varphi_{1} + \varphi_{3}/(\omega^{2}\rho_{a}), \\ \text{where} \quad w_{j} &= 2(f_{j} \circ p), \quad \varphi_{j} = (g_{j} \circ p), \quad \varphi_{j}' = (g_{j} \circ p)', \quad j = 1, 2, 3, \quad \text{and} \quad \tilde{\tau}' := (\tilde{\tau}_{1}', \tilde{\tau}_{2}')^{\top}, \\ \tilde{\nu}' := (\tilde{\nu}_{1}', \tilde{\nu}_{2}')^{\top}. \end{split}$$

To avoid calculating the derivative of the Jacobi G in numerical discretization, we transform the parametrized integral equation (5.1) to

$$\begin{split} w_{1} &= -\mu\kappa_{p}^{2}\tilde{\nu}^{\top}S_{\kappa_{p}}\left[\mathsf{nn}^{\top}\tilde{\varphi}_{1};p\right]\tilde{\nu} + \mu\tilde{\nu}^{\top}K_{\kappa_{p}}\left[\mathsf{n}^{\perp}\tilde{\varphi}_{1}' + \mathsf{n}^{\perp'}\tilde{\varphi}_{1};p\right] - \mu\tilde{\nu}^{\top}H_{\kappa_{p}}\left[\mathsf{n}\tilde{\varphi}_{1}' + \mathsf{n}'\tilde{\varphi}_{1};p\right] \\ &+ \mu\kappa_{s}^{2}\tilde{\nu}^{\top}S_{\kappa_{s}}\left[\mathsf{n}^{\perp}\mathsf{n}^{\top}\tilde{\varphi}_{2};p\right]\tilde{\nu} + \mu\tilde{\nu}^{\top}K_{\kappa_{s}}\left[\mathsf{n}\tilde{\varphi}_{2}' + \mathsf{n}'\tilde{\varphi}_{2};p\right] + \mu\tilde{\nu}^{\top}H_{\kappa_{s}}\left[\mathsf{n}^{\perp}\tilde{\varphi}_{2}' + \mathsf{n}^{\perp'}\tilde{\varphi}_{2};p\right] \\ &- (\lambda + \mu)\kappa_{p}^{2}S_{\kappa_{p}}\left[\tilde{\varphi}_{1}G^{2};p\right] + S_{\kappa_{a}}\left[\tilde{\varphi}_{3}G^{2};p\right] + \mu(\tilde{\nu}\cdot\mathsf{n}^{\perp'})\tilde{\varphi}_{1}/G + \mu(\tilde{\nu}\cdot\mathsf{n}')\tilde{\varphi}_{2}/G + \mu\tilde{\varphi}_{2}', \\ w_{2} &= -\kappa_{p}^{2}\tilde{\tau}^{\top}S_{\kappa_{p}}\left[\mathsf{nn}^{\top}\tilde{\varphi}_{1};p\right]\tilde{\nu} + \tilde{\tau}^{\top}K_{\kappa_{p}}\left[\mathsf{n}^{\perp}\tilde{\varphi}_{1}' + \mathsf{n}^{\perp'}\tilde{\varphi}_{1};p\right] - \tilde{\tau}^{\top}H_{\kappa_{p}}\left[\mathsf{n}\tilde{\varphi}_{1}' + \mathsf{n}'\tilde{\varphi}_{1};p\right] \\ &+ \kappa_{s}^{2}\tilde{\tau}^{\top}S_{\kappa_{s}}\left[\mathsf{n}^{\perp}\mathsf{n}^{\top}\tilde{\varphi}_{2};p\right]\tilde{\nu} + \tilde{\tau}^{\top}K_{\kappa_{s}}\left[\mathsf{n}\tilde{\varphi}_{2}' + \mathsf{n}'\tilde{\varphi}_{2};p\right] + \tilde{\tau}^{\top}H_{\kappa_{s}}\left[\mathsf{n}^{\perp}\tilde{\varphi}_{2}' + \mathsf{n}^{\perp'}\tilde{\varphi}_{2};p\right] \\ &+ (\tilde{\tau}\cdot\mathsf{n}^{\perp'})\tilde{\varphi}_{1}/G + \tilde{\varphi}_{1}' + (\tilde{\tau}\cdot\mathsf{n}')\tilde{\varphi}_{2}/G, \\ w_{3} &= K_{\kappa_{p}}\left[\tilde{\varphi}_{1}G^{2};p\right] + H_{\kappa_{s}}\left[\tilde{\varphi}_{2}G^{2};p\right] - K_{\kappa_{a}}\left[\tilde{\varphi}_{3}G^{2};p\right]/(\omega^{2}\rho_{a}) + \tilde{\varphi}_{1}G + \tilde{\varphi}_{3}G/(\omega^{2}\rho_{a}), \\ \text{where } \tilde{\varphi}_{l} &= \varphi_{l}/G, \ l = 1, 2, 3, \ \mathsf{n}' = \left(p_{2}'', -p_{1}''\right)^{\top}, \ \text{and } \mathsf{n}^{\perp'} = \left(p_{1}'', p_{2}''\right)^{\top}. \end{split}$$

5.2. Discretization

As in [7, section 3.5], the kernel \widetilde{M} and \widetilde{K} of the parametrized single-layer and normal derivative integral operators can be written in the form of

$$\widetilde{M}(t,\varsigma;\kappa) = \widetilde{M}_1(t,\varsigma;\kappa) \ln\left(4\sin^2\frac{t-\varsigma}{2}\right) + \widetilde{M}_2(t,\varsigma;\kappa),$$

$$\widetilde{K}(t,\varsigma;\kappa) = \widetilde{K}_1(t,\varsigma;\kappa) \ln\left(4\sin^2\frac{t-\varsigma}{2}\right) + \widetilde{K}_2(t,\varsigma;\kappa),$$

where

$$\begin{split} \widetilde{M}_1(t,\varsigma;\kappa) &= -\frac{1}{2\pi} J_0(\kappa|p(t) - p(\varsigma)|), \\ \widetilde{M}_2(t,\varsigma;\kappa) &= \widetilde{M}(t,\varsigma;\kappa) - \widetilde{M}_1(t,\varsigma;\kappa) \ln\left(4\sin^2\frac{t-\varsigma}{2}\right), \\ \widetilde{K}_1(t,\varsigma;\kappa) &= \frac{\kappa}{2\pi} \mathsf{n}(t) \cdot \left[p(t) - p(\varsigma)\right] \frac{J_1(\kappa|p(t) - p(\varsigma)|)}{|p(t) - p(\varsigma)|}, \\ \widetilde{K}_2(t,\varsigma;\kappa) &= \widetilde{K}(t,\varsigma;\kappa) - \widetilde{K}_1(t,\varsigma;\kappa) \ln\left(4\sin^2\frac{t-\varsigma}{2}\right), \end{split}$$

and the diagonal terms are given as

$$\begin{split} \widetilde{M}_1(t,t;\kappa) &= -\frac{1}{2\pi}, & \widetilde{M}_2(t,t;\kappa) &= \frac{\mathrm{i}}{2} - \frac{E_\mathrm{c}}{\pi} - \frac{1}{\pi} \ln\left(\frac{\kappa}{2}G(t)\right), \\ \widetilde{K}_1(t,t;\kappa) &= 0, & \widetilde{K}_2(t,t;\kappa) &= \frac{1}{2\pi} \frac{\mathrm{n}(t) \cdot p''(t)}{|p'(t)|^2}, \end{split}$$

with the Euler constant $E_c = 0.57721 \cdots$.

For the kernel \widetilde{H} of parametrized tangential derivative integral operator, analogously to [8], we split the kernel in the form

$$\widetilde{H}(t,\varsigma;\kappa) = \widetilde{H}_1(t,\varsigma;\kappa) \frac{1}{\sin(\varsigma-t)} + \widetilde{H}_2(t,\varsigma;\kappa) \ln\left(4\sin^2\frac{t-\varsigma}{2}\right) + \widetilde{H}_3(t,\varsigma;\kappa),$$

where

$$\begin{split} \widetilde{H}_1(t,\varsigma;\kappa) &= \frac{1}{\pi} \mathsf{n}(t)^\perp \cdot \left[p(\varsigma) - p(t) \right] \frac{\sin(\varsigma - t)}{|p(t) - p(\varsigma)|^2}, \\ \widetilde{H}_2(t,\varsigma;\kappa) &= \frac{\kappa}{2\pi} \mathsf{n}(t)^\perp \cdot \left[p(t) - p(\varsigma) \right] \frac{J_1(\kappa|p(t) - p(\varsigma)|)}{|p(t) - p(\varsigma)|}, \\ \widetilde{H}_3(t,\varsigma;\kappa) &= \widetilde{H}(t,\varsigma;\kappa) - \widetilde{H}_1(t,\varsigma;\kappa) \frac{1}{\sin(\varsigma - t)} - \widetilde{H}_2(t,\varsigma;\kappa) \ln\left(4\sin^2\frac{t - \varsigma}{2}\right) \end{split}$$

turn out to be analytic with the diagonal terms

$$\widetilde{H}_1(t,t;\kappa) = \frac{1}{\pi}, \quad \widetilde{H}_2(t,t;\kappa) = 0, \quad \widetilde{H}_3(t,t;\kappa) = 0.$$

Let $\varsigma_j^{(n)} := \pi j/n$, $j = 0, \dots, 2n-1$ be an equidistant set of quadrature nodes. For the integrals of weakly singular and singular, by making use of quadrature rule in [7, equation (3.93)] and our previous work [8, equation (4.6)], we employ the following quadrature rules

$$\int_{0}^{2\pi} \ln\left(4\sin^{2}\frac{t-\varsigma}{2}\right) Q(t,\varsigma) f(\varsigma) d\varsigma \approx \sum_{j=0}^{2n-1} R_{j}^{(n)}(t) Q(t,\varsigma_{j}^{(n)}) f(\varsigma_{j}^{(n)}), \tag{5.3}$$

$$\int_{0}^{2\pi} \frac{1}{\sin(\varsigma - t)} Q(t, \varsigma) f(\varsigma) d\varsigma \approx \sum_{i=0}^{2n-1} T_{j}^{(n)}(t) Q(t, \varsigma_{j}^{(n)}) f(\varsigma_{j}^{(n)}), \tag{5.4}$$

where the function Q is required to be continuous, and the quadrature weights are given by

$$R_{j}^{(n)}(t) = -\frac{2\pi}{n} \sum_{m=1}^{n-1} \frac{1}{m} \cos\left[m(t-\varsigma_{j}^{(n)})\right] - \frac{\pi}{n^{2}} \cos\left[n(t-\varsigma_{j}^{(n)})\right]$$

$$T_{j}^{(n)}(t) = \begin{cases} -\frac{2\pi}{n} \sum_{m=0}^{(n-3)/2} \sin\left[(2m+1)(t-\varsigma_{j}^{(n)})\right] - \frac{\pi}{n} \sin\left[n(t-\varsigma_{j}^{(n)})\right], & n=1,3,5,\cdots, \\ -\frac{2\pi}{n} \sum_{m=0}^{n/2-1} \sin\left[(2m+1)(t-\varsigma_{j}^{(n)})\right], & n=2,4,6,\cdots. \end{cases}$$

On the other hand, with the help of trapezoidal rule

$$\int_{0}^{2\pi} f(\varsigma) d\varsigma \approx \frac{\pi}{n} \sum_{i=0}^{2n-1} f(\varsigma_{i}^{(n)})$$
 (5.5)

and Lagrange bases

$$\mathcal{L}_m(\varsigma) = \frac{1}{2n} \left\{ 1 + 2 \sum_{k=1}^{n-1} \cos k(\varsigma - \varsigma_m^{(n)}) + \cos n(\varsigma - \varsigma_m^{(n)}) \right\}$$

for the trigonometric interpolation, we design the following quadrature rules for the integration with derivatives of a function involved

$$\int_{0}^{2\pi} Q(t,\varsigma)f'(\varsigma)d\varsigma \approx \frac{\pi}{n} \sum_{j=0}^{2n-1} \sum_{m=0}^{2n-1} d_{m-j}^{(n)} Q(t,\varsigma_{m}^{(n)}) f(\varsigma_{j}^{(n)}),$$
(5.6)

$$\int_{0}^{2\pi} \ln\left(4\sin^{2}\frac{t-\varsigma}{2}\right) Q(t,\varsigma) f'(\varsigma) d\varsigma \approx \sum_{j=0}^{2n-1} \sum_{m=0}^{2n-1} d_{m-j}^{(n)} R_{m}^{(n)}(t) Q(t,\varsigma_{m}^{(n)}) f(\varsigma_{j}^{(n)}),$$
(5.7)

$$\int_{0}^{2\pi} \frac{1}{\sin(\varsigma - t)} Q(t, \varsigma) f'(\varsigma) d\varsigma \approx \sum_{j=0}^{2n-1} \sum_{m=0}^{2n-1} d_{m-j}^{(n)} T_{m}^{(n)}(t) Q(t, \varsigma_{m}^{(n)}) f(\varsigma_{j}^{(n)}),$$
(5.8)

where we have set $d_{m-j}^{(n)} = \mathcal{L}'_{j}(\varsigma_{m}^{(n)})$, and the quadrature weights are given by

$$d_{j}^{(n)} = egin{cases} rac{(-1)^{j}}{2}\cotrac{j\pi}{2n}, & j = \pm 1, \cdots, \pm 2n-1, \ 0, & j = 0. \end{cases}$$

To obtain a Nyström-type discretization, we use the following combination

$$\tilde{\varphi}_l^{(n)}(\varsigma) = \sum_{i=0}^{2n-1} \Upsilon_j^{(l)} \mathcal{L}_j(\varsigma)$$

with unknowns $\Upsilon_j^{(l)} := \tilde{\varphi}_l(\varsigma_j^{(n)})$ as finite dimensional approximation of the densities $\tilde{\varphi}_l$, l = 1, 2, 3. Then, the derivative $\tilde{\varphi}_l'$ can be approximated by

$$\tilde{\varphi}_{l}^{'(n)}(\varsigma) = \sum_{i=0}^{2n-1} \Upsilon_{j}^{(l)} \mathcal{L}_{j}'(\varsigma).$$

Hence, in view of the quadrature rules (5.3)–(5.8), the full discretization of (5.2) can be deduced as a linear system with unknowns $\Upsilon_i^{(l)}$, $l=1,2,3,j=0,1,\cdots,2n-1$.

6. Reconstruction methods

In this section, we introduce the iterative methods and the algorithms for the phased and phaseless IAEIP.

6.1. Iterative method for the phased IAEIP

We assume that the field equations are given in (3.12), and the data equation is given by

$$S_{\kappa_n}^{\infty}[g_3] = u_{\infty}.$$

Thus, the field equations and data equation can be reformulated as the parametrized integral equation (5.1) and

$$S_{\kappa_n}^{\infty}[\varphi_3 G; p] = w_{\infty},\tag{6.1}$$

where $w_{\infty} = u_{\infty} \circ p$.

In the reconstruction process, when an approximation of the boundary Γ_D is available, the field equation (5.1) are solved for the densities φ_l , l=1,2,3. Once the approximated densities φ_l are computed, the update of the boundary Γ_D can be obtained by solving a linearized data equation for (6.1) with respect to Γ_D .

6.1.1. Iterative scheme. The linearization of (6.1) with respect to a given p requires the Fréchet derivative of the parameterized integral operator S_{κ}^{∞} , which can be easily computed and is given by

$$\left(S_{\kappa}^{\infty'}[\vartheta;p]q\right)(t) = -i\kappa\gamma_{\kappa} \int_{0}^{2\pi} e^{-i\kappa\hat{x}(t)\cdot p(\varsigma)}\hat{x}(t) \cdot q(\varsigma)\vartheta(\varsigma)d\varsigma
= -i\kappa\gamma_{\kappa} \int_{0}^{2\pi} \exp\left(-i\kappa\left(c_{1}\cos t + c_{2}\sin t + r(\varsigma)\cos(t - \varsigma)\right)\right)
\cdot \left(\Delta c_{1}\cos t + \Delta c_{2}\sin t + \Delta r(\varsigma)\cos(t - \varsigma)\right)\vartheta(\varsigma)d\varsigma,$$
(6.2)

where $q(\varsigma) = (\Delta c_1, \Delta c_2) + \Delta r(\varsigma)(\cos \varsigma, \sin \varsigma)$ is denoted as the update of the boundary Γ_D . Then, the linearization of (6.1) leads to

$$S_{\kappa_a}^{\infty'}[\varphi_3 G; p]q = w, \tag{6.3}$$

where

$$w := w_{\infty} - S_{\kappa_0}^{\infty} [\varphi_3 G; p].$$

Here, we apply the regularization techniques to overcome the ill-posedness of the linearized data equation (6.3). In order to apply Tikhonov regularization, the injectivity and denseness of the range for operator $S_{\kappa_a}^{\infty}$ are proved in [18, theorems 4.1 and 4.2] with the assumption that k_a^2 is not an interior Neumann eigenvalue for the negative Laplacian in D.

Table 1. Parametrization of the exact boundary curves.

Туре	Parametrization
Apple-shaped	$p_D(t) = \frac{0.55(1+0.9\cos t + 0.1\sin 2t)}{1+0.75\cos t}(\cos t, \sin t), t \in [0, 2\pi]$
Peanut-shaped	$p_D(t) = 0.65\sqrt{0.25\cos^2 t + \sin^2 t}(\cos t, \sin t), t \in [0, 2\pi]$

These properties imply that Tikhonov regularization combined with the discrepancy principle is a regularizing scheme. Analogously to [18], we can control the size of D such that $k_{\rm a}^2, k_{\rm p}^2, k_{\rm s}^2$ are not interior Dirichlet eigenvalues and $k_{\rm a}^2$ is not a interior Neumann eigenvalue to ensure the existence and uniqueness of a solution to the boundary integral equations involved in the algorithm. We refer to [20, equation (3.5)] for an interrelation between the iterative scheme of Johannson and Sleeman [25] and the traditional Newton iterations [14, 28, 31]. Theoretically, the convergence of regularized Newton iterations for inverse obstacle scattering problems has not been completely settled due to its highly ill-posedness and it remains an open problem [7, 20, 31]. We refer to [15, 42] for the promising convergence results of regularized Newton iterations for inverse obstacle scattering problems.

As usual for iterative algorithms, the stopping criteria is necessary to justify the convergence numerically. With regard to our iterative procedure, the relative error estimator is chosen as follows

$$E_{k} := \frac{\left\| w_{\infty} - S_{\kappa_{a}}^{\infty} [\varphi_{3} G; p^{(k)}] \right\|_{L^{2}}}{\left\| w_{\infty} \right\|_{L^{2}}} \leqslant \epsilon \tag{6.4}$$

for some sufficiently small parameter $\epsilon > 0$ depending on the noise level, where $p^{(k)}$ is the kth approximation of the boundary Γ_D .

We are now in a position to present the iterative algorithm for the inverse obstacle scattering problem with phased far-field data as algorithm I.

Algorithm I. Iterative algorithm for the phased IAEIP.

Step 1 Send an incident plane wave u^{inc} with a fixed wave number κ_a and a fixed incident direction $d \in \Omega$, and then collect the corresponding far-field data u_{∞} for the scatterer D:

Step 2 Select an initial star-like curve $\Gamma^{(0)}$ for the boundary Γ_D and the error tolerance ϵ . Set k=0;

Step 3 For the curve $\Gamma^{(k)}$, compute the densities φ_l , l = 1, 2, 3 from (5.1);

Step 4 Solve (6.3) to obtain the updated approximation $\Gamma^{(k+1)} := \Gamma^{(k)} + q$ and evaluate the error E_{k+1} defined in (6.4);

Step 5 If $E_{k+1} \ge \epsilon$, then set k = k+1 and go to Step 3. Otherwise, the current approximation $\Gamma^{(k+1)}$ is taken to be the final reconstruction of Γ_D .

6.1.2. Discretization. We use the Nyström-type method which is described in section 5 for the full discretizations of (5.1). Now we discuss the discretization of the linearized equation (6.3) and obtain the update by using the least squares with Tikhonov regularization [31]. As for a finite dimensional space to approximate the radial function r and its update Δr , we choose the space of trigonometric polynomials of the form

$$\Delta r(\varsigma) = \sum_{m=0}^{M} \alpha_m \cos m\varsigma + \sum_{m=1}^{M} \beta_m \sin m\varsigma$$

where the integer M > 1 is the truncation number. For simplicity, we reformulate the equation (6.3) by introducing the following definitions

$$\begin{split} L_1(t,\varsigma;\varphi) &:= -\mathrm{i}\kappa_\mathrm{a}\gamma_{\kappa_\mathrm{a}} \exp\left\{-\mathrm{i}\kappa_\mathrm{a} \big(c_1\cos t + c_2\sin t + r(\varsigma)\cos(t-\varsigma)\big)\right\} \cos t\,\varphi(\varsigma), \\ L_2(t,\varsigma;\varphi) &:= -\mathrm{i}\kappa_\mathrm{a}\gamma_{\kappa_\mathrm{a}} \exp\left\{-\mathrm{i}\kappa_\mathrm{a} \big(c_1\cos t + c_2\sin t + r(\varsigma)\cos(t-\varsigma)\big)\right\} \sin t\,\varphi(\varsigma), \\ L_{3,m}(t,\varsigma;\varphi) &:= -\mathrm{i}\kappa_\mathrm{a}\gamma_{\kappa_\mathrm{a}} \exp\left\{-\mathrm{i}\kappa_\mathrm{a} \big(c_1\cos t + c_2\sin t + r(\varsigma)\cos(t-\varsigma)\big)\right\} \cos(t-\varsigma) \cos m\varsigma\,\varphi(\varsigma), \\ L_{4,m}(t,\varsigma;\varphi) &:= -\mathrm{i}\kappa_\mathrm{a}\gamma_{\kappa_\mathrm{a}} \exp\left\{-\mathrm{i}\kappa_\mathrm{a} \big(c_1\cos t + c_2\sin t + r(\varsigma)\cos(t-\varsigma)\big)\right\} \cos(t-\varsigma) \sin m\varsigma\,\varphi(\varsigma). \end{split}$$

Then, by combining (6.2) and (6.3) together and using trapezoidal rule (5.5), we get the discretized linear system

$$\sum_{l=1}^{2} B_{l}^{c}(\varsigma_{i}^{(\tilde{n})}) \Delta c_{l} + \sum_{m=0}^{M} \alpha_{m} B_{1,m}^{r}(\varsigma_{i}^{(\tilde{n})}) + \sum_{m=1}^{M} \beta_{m} B_{2,m}^{r}(\varsigma_{i}^{(\tilde{n})}) = w(\varsigma_{i}^{(\tilde{n})})$$
(6.5)

to determine the real coefficients $\Delta c_1, \Delta c_2, \alpha_m$ and β_m , where $\varsigma_i^{(\tilde{n})} := \pi i / \tilde{n}, \ i = 0, 1, \dots, 2\tilde{n} - 1$ are the far-field observation points in $[0, 2\pi]$,

$$B_l^c(\varsigma_i^{(\tilde{n})}) = \frac{\pi}{n} \sum_{i=0}^{2n-1} L_l(\varsigma_i^{(\tilde{n})}, \varsigma_j^{(n)}; \varphi_3 G)$$

for l = 1, 2, and

$$B^{r}_{1,m}(\varsigma_{i}^{(\tilde{n})}) = \frac{\pi}{n} \sum_{j=0}^{2n-1} L_{3,m}(\varsigma_{i}^{(\tilde{n})},\varsigma_{j}^{(n)};\varphi_{3}G), \qquad B^{r}_{2,m}(\varsigma_{i}^{(\tilde{n})}) = \frac{\pi}{n} \sum_{j=0}^{2n-1} L_{4,m}(\varsigma_{i}^{(\tilde{n})},\varsigma_{j}^{(n)};\varphi_{3}G).$$

In general, $2M + 1 \ll 2\tilde{n}$, and due to the ill-posedness, the overdetermined system (6.5) is solved via the Tikhonov regularization. Hence the linear system (6.5) is reformulated into minimizing the following function

$$\sum_{i=0}^{2\tilde{n}-1} \left| \sum_{l=1}^{2} B_{l}^{c}(\varsigma_{i}^{(\tilde{n})}) \Delta c_{l} + \sum_{m=0}^{M} \alpha_{m} B_{1,m}^{r}(\varsigma_{i}^{(\tilde{n})}) + \sum_{m=1}^{M} \beta_{m} B_{2,m}^{r}(\varsigma_{i}^{(\tilde{n})}) - w(\varsigma_{i}^{(\tilde{n})}) \right|^{2} + \lambda \left(|\Delta c_{1}|^{2} + |\Delta c_{2}|^{2} + 2\pi \left[\alpha_{0}^{2} + \frac{1}{2} \sum_{m=1}^{M} (1 + m^{2})^{2} (\alpha_{m}^{2} + \beta_{m}^{2}) \right] \right)$$
(6.6)

with H^2 penalty term, where $\lambda > 0$ is a regularization parameter. It is easy to show that the minimizer of (6.6) is the solution of the system

$$(\lambda \widetilde{I} + \Re(\widetilde{B}^*\widetilde{B}))\xi = \Re(\widetilde{B}^*\widetilde{w}), \tag{6.7}$$

where

$$\widetilde{B} = (B_1^c, B_2^c, B_{1,0}^r, \cdots, B_{1,M}^r, B_{2,1}^r, \cdots, B_{2,M}^r)_{(2\tilde{n}) \times (2M+3)},$$

$$\xi = (\Delta c_1, \Delta c_2, \alpha_0, \cdots, \alpha_M, \beta_1, \cdots, \beta_M)^\top,$$

$$\widetilde{I} = \text{diag}\{1, 1, 2\pi, \pi(1+1^2)^2, \cdots, \pi(1+M^2)^2, \pi(1+1^2)^2, \cdots, \pi(1+M^2)^2\},$$

$$\widetilde{w} = (w(\varsigma_0^{(\tilde{n})}), \cdots, w(\varsigma_{2\tilde{n}-1}^{(\tilde{n})}))^\top.$$

Thus, we obtain the new approximation

$$p^{\text{new}}(\hat{x}) = (c + \Delta c) + (r(\hat{x}) + \Delta r(\hat{x}))\hat{x}.$$

6.2. Iterative method for the phaseless IAEIP

To incorporate the reference ball, we find the solution of (2.6) with D replaced by $D \cup B$ in the form of single-layer potentials with densities $g_{1,\sigma}$, $g_{2,\sigma}$ and $g_{3,\sigma}$:

$$\phi(x) = \sum_{\sigma} \int_{\Gamma_{\sigma}} \Phi(x, y; \kappa_{p}) g_{1,\sigma}(y) ds(y), \tag{6.8}$$

$$\psi(x) = \sum_{\sigma} \int_{\Gamma_{\sigma}} \Phi(x, y; \kappa_{s}) g_{2,\sigma}(y) ds(y), \tag{6.9}$$

$$u^{s}(x) = \sum_{\sigma} \int_{\Gamma_{\sigma}} \Phi(x, y; \kappa_{a}) g_{3,\sigma}(y) \mathrm{d}s(y), \tag{6.10}$$

for $x \in \mathbb{R}^2 \setminus \Gamma_{D \cup B}$, where $\sigma = D, B$.

Furthermore, we introduce following integral operators, i.e.

$$\begin{split} S_{\kappa}^{\sigma,\varrho}[g](x) &= 2 \int_{\Gamma_{\sigma}} \Phi(x,y;\kappa) g(y) \mathrm{d}s(y), \quad x \in \Gamma_{\varrho}, \\ S_{\kappa,\sigma}^{\infty}[g](\hat{x}) &= \gamma_{\kappa} \int_{\Gamma_{\sigma}} \mathrm{e}^{-\mathrm{i}\kappa \hat{x} \cdot y} g(y) \mathrm{d}s(y), \quad \hat{x} \in \Omega, \\ K_{\kappa}^{\sigma,\varrho}[g](x) &= 2 \int_{\Gamma_{\sigma}} \frac{\partial \Phi(x,y;\kappa)}{\partial \nu(x)} g(y) \mathrm{d}s(y), \quad x \in \Gamma_{\varrho}, \\ H_{\kappa}^{\sigma,\varrho}[g](x) &= 2 \int_{\Gamma_{\sigma}} \frac{\partial \Phi(x,y;\kappa)}{\partial \tau(x)} g(y) \mathrm{d}s(y), \quad x \in \Gamma_{\varrho}, \end{split}$$

where $\varrho = D, B$. Then, letting $x \in \mathbb{R}^2 \setminus \overline{D \cup B}$ tend to boundaries Γ_D and Γ_B respectively in (6.8)–(6.10), and making use of the jump relation of the single-layer potentials and the boundary condition of (2.6) for $\Gamma_{D \cup B}$, we can readily deduce the following field equations in the operator form on Γ_D :

$$2f_{1} = -\mu \kappa_{p}^{2} \nu_{D}^{\top} S_{\kappa_{p}}^{D,D} \left[\nu_{D} \nu_{D}^{\top} g_{1,D} \right] \nu_{D} + \mu \nu_{D}^{\top} K_{\kappa_{p}}^{D,D} \left[\tau_{D} \partial_{\tau_{D}} g_{1,D} + g_{1,D} \partial_{\tau_{D}} \tau_{D} \right]$$

$$- \mu \nu_{D}^{\top} H_{\kappa_{p}}^{D,D} \left[\nu_{D} \partial_{\tau_{D}} g_{1,D} + g_{1,D} \partial_{\tau_{D}} \nu_{D} \right] + \mu \kappa_{s}^{2} \nu_{D}^{\top} S_{\kappa_{s}}^{D,D} \left[\tau_{D} \nu_{D}^{\top} g_{2,D} \right] \nu_{D}$$

$$+ \mu \nu_{D}^{\top} K_{\kappa_{s}}^{D,D} \left[\nu_{D} \partial_{\tau_{D}} g_{2,D} + g_{2,D} \partial_{\tau_{D}} \nu_{D} \right] + \mu \nu_{D}^{\top} H_{\kappa_{s}}^{D,D} \left[\tau_{D} \partial_{\tau_{D}} g_{2,D} + g_{2,D} \partial_{\tau_{D}} \tau_{D} \right]$$

$$+ \mu \nu_{D} \cdot \partial_{\nu_{D}} \nabla S_{\kappa_{p}}^{B,D} \left[g_{1,B} \right] + \mu \nu_{D} \cdot \partial_{\nu_{D}} \mathbf{curl} S_{\kappa_{s}}^{B,D} \left[g_{2,B} \right] - (\lambda + \mu) \kappa_{p}^{2} \left(S_{\kappa_{p}}^{D,D} \left[g_{1,D} \right] + S_{\kappa_{p}}^{B,D} \left[g_{1,B} \right] \right)$$

$$+ S_{\kappa_{s}}^{D,D} \left[g_{3,D} \right] + S_{\kappa_{s}}^{B,D} \left[g_{3,B} \right] + \mu (\nu_{D} \cdot \partial_{\tau_{D}} \tau_{D}) g_{1,D} + \mu (\nu_{D} \cdot \partial_{\tau_{D}} \nu_{D}) g_{2,D} + \mu \partial_{\tau_{D}} g_{2,D},$$

$$(6.11)$$

$$2f_{2} = -\kappa_{p}^{2} \tau_{D}^{\top} S_{\kappa_{p}}^{D,D} \left[\nu_{D} \nu_{D}^{\top} g_{1,D} \right] \nu_{D} + \tau_{D}^{\top} K_{\kappa_{p}}^{D,D} \left[\tau_{D} \partial_{\tau_{D}} g_{1,D} + g_{1,D} \partial_{\tau_{D}} \tau_{D} \right]$$

$$- \tau_{D}^{\top} H_{\kappa_{p}}^{D,D} \left[\nu_{D} \partial_{\tau_{D}} g_{1,D} + g_{1,D} \partial_{\tau_{D}} \nu_{D} \right] + \kappa_{s}^{2} \tau_{D}^{\top} S_{\kappa_{s}}^{D,D} \left[\tau_{D} \nu_{D}^{\top} g_{2,D} \right] \nu_{D}$$

$$+ \tau_{D}^{\top} K_{\kappa_{s}}^{D,D} \left[\nu_{D} \partial_{\tau_{D}} g_{2,D} + g_{2,D} \partial_{\tau_{D}} \nu_{D} \right] + \tau_{D}^{\top} H_{\kappa_{s}}^{D,D} \left[\tau_{D} \partial_{\tau_{D}} g_{2,D} + g_{2,D} \partial_{\tau_{D}} \tau_{D} \right]$$

$$+ \tau_{D} \cdot \partial_{\nu_{D}} \nabla S_{\kappa_{p}}^{B,D} \left[g_{1,B} \right] + \tau_{D} \cdot \partial_{\nu_{D}} \mathbf{curl} S_{\kappa_{s}}^{B,D} \left[g_{2,B} \right]$$

$$+ (\tau_{D} \cdot \partial_{\tau_{D}} \tau_{D}) g_{1,D} + \partial_{\tau_{D}} g_{1,D} + (\tau_{D} \cdot \partial_{\tau_{D}} \nu_{D}) g_{2,D},$$

$$(6.12)$$

$$2f_{3} = K_{\kappa_{p}}^{D,D}[g_{1,D}] + K_{\kappa_{p}}^{B,D}[g_{1,B}] + H_{\kappa_{s}}^{D,D}[g_{2,D}] + H_{\kappa_{s}}^{B,D}[g_{2,B}] - (K_{\kappa_{a}}^{D,D}[g_{3,D}] + K_{\kappa_{a}}^{B,D}[g_{3,B}])/(\omega^{2}\rho_{a}) + g_{1,D} + g_{3,D}/(\omega^{2}\rho_{a}),$$

$$(6.13)$$

and on Γ_B the field equations are the same as above with superscript/subscript D and B interchanged. The phaseless data equation is given by

$$\left|\sum_{\sigma} S_{\kappa_{\mathbf{a}},\sigma}^{\infty}[g_{3,\sigma}]\right|^2 = |u_{\infty}|^2. \tag{6.14}$$

In the reconstruction process, the field equations are solved for $g_{1,\sigma}$, $g_{2,\sigma}$ and $g_{3,\sigma}$ with an approximation of the boundary Γ_D . Then, by keeping $g_{1,\sigma}$, $g_{2,\sigma}$ and $g_{3,\sigma}$ fixed, the update of the boundary Γ_D can be obtained by linearizing (6.14) with respect to Γ_D .

6.2.1. Parametrization and iterative scheme. For simplicity, the boundary Γ_D and Γ_B are assumed to be starlike curves with the parametrized form

$$\Gamma_D = \{ p_D(\hat{x}) = c + r(\hat{x})\hat{x}; \ c = (c_1, c_2)^\top, \ \hat{x} \in \Omega \},$$

$$\Gamma_B = \{ p_B(\hat{x}) = b + R\hat{x}; \ b = (b_1, b_2)^\top, \ \hat{x} \in \Omega \},$$

where $\Omega = \{\hat{x}(t) = (\cos t, \sin t)^{\top}; \ 0 \le t < 2\pi\}$. We assume $G_D(\varsigma) := |p'(\varsigma)| = \sqrt{(r'(\varsigma))^2 + r^2(\varsigma)}$ and $G_B = R$ denoted as the Jacobian of the transformation.

Now, we reformulate the phaseless data equation (6.14) as the parametrized integral equations

$$\left|\sum_{\sigma} S_{\kappa_{a},\sigma}^{\infty} [\varphi_{3,\sigma} G_{\sigma}; p_{\sigma}]\right|^{2} = |u_{\infty}|^{2}, \tag{6.15}$$

where $\varphi_{3,\sigma} = g_3 \circ p_{\sigma}$, $\sigma = D, B$. By recalling the Fréchet derivative operator $S_{\kappa}^{\infty}[p;\varphi]q$ in (6.2), the linearization of (6.15) leads to

$$2\Re\left(\overline{\sum_{\sigma} S_{\kappa_{a},\sigma}^{\infty}[\varphi_{3,\sigma}G_{\sigma};p_{\sigma}]}S_{\kappa_{a}}^{\infty'}[\varphi_{3,D}G_{D};p_{D}]q\right) = \breve{w},\tag{6.16}$$

where

$$reve{w} := |u_\infty|^2 - igg| \sum_\sigma S^\infty_{\kappa_\mathrm{a},\sigma} [arphi_{3,\sigma} G_\sigma; p_\sigma] igg|^2.$$

Again, with regard to our iterative procedure, the relative error estimator is chosen as following

$$E_{k} := \frac{\left\| |u_{\infty}|^{2} - \left| S_{\kappa_{a},D}^{\infty}[\varphi_{3,D}G_{D}; p_{D}^{(k)}] + S_{\kappa_{a},B}^{\infty}[\varphi_{3,B}G_{B}; p_{B}] \right|^{2} \right\|_{L^{2}}}{\left\| |u_{\infty}|^{2} \right\|_{L^{2}}} \leqslant \epsilon \tag{6.17}$$

for some sufficiently small parameter $\epsilon > 0$ depending on the noise level, where $p_D^{(k)}$ is the kth approximation of the boundary Γ_D .

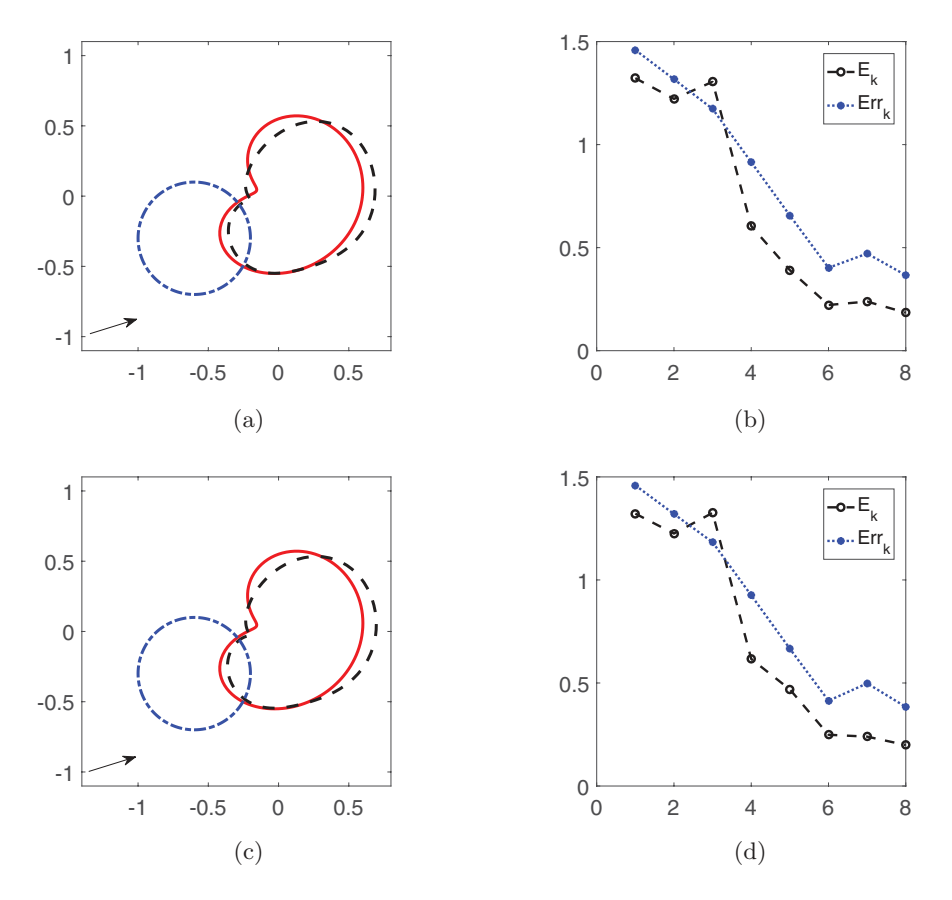


Figure 2. Reconstructions of an apple-shaped obstacle with phased data at different levels of noise (see Example 1). The initial guess is given by $(c_1^{(0)},c_2^{(0)})=(-0.6,-0.3), r^{(0)}=0.4$ and the incident angle $\theta=\pi/8$. (a) Reconstruction with 1% noise, $\epsilon=0.2$. (b) Relative error with 1% noise. (c) Reconstruction with 5% noise, $\epsilon=0.2$. (d) Relative error with 5% noise.

The iterative algorithm for the phaseless IAEIP is given by algorithm II.

Algorithm II. Iterative algorithm for the phaseless IAEIP.

Step 1 Send an incident plane wave u^{inc} with a fixed wave number κ_a and a fixed incident direction $d \in \Omega$, and then collect the corresponding far-field data u_{∞} for the scatterer $D \cup B$;

Step 2 Select an initial star-like curve $\Gamma^{(0)}$ for the boundary Γ_D and the error tolerance ϵ . Set k=0;

Step 3 For the curve $\Gamma^{(k)}$, compute the densities $\varphi_{1,\sigma}$, $\varphi_{2,\sigma}$ and $\varphi_{3,\sigma}$ from field equations;

Step 4 Solve (6.16) to obtain the updated approximation $\Gamma^{(k+1)} := \Gamma^{(k)} + q$ and evaluate the error E_{k+1} defined in (6.17);

Step 5 If $E_{k+1} \ge \epsilon$, then set k = k+1 and go to Step 3. Otherwise, the current approximation $\Gamma^{(k+1)}$ is served as the final reconstruction of Γ_D .

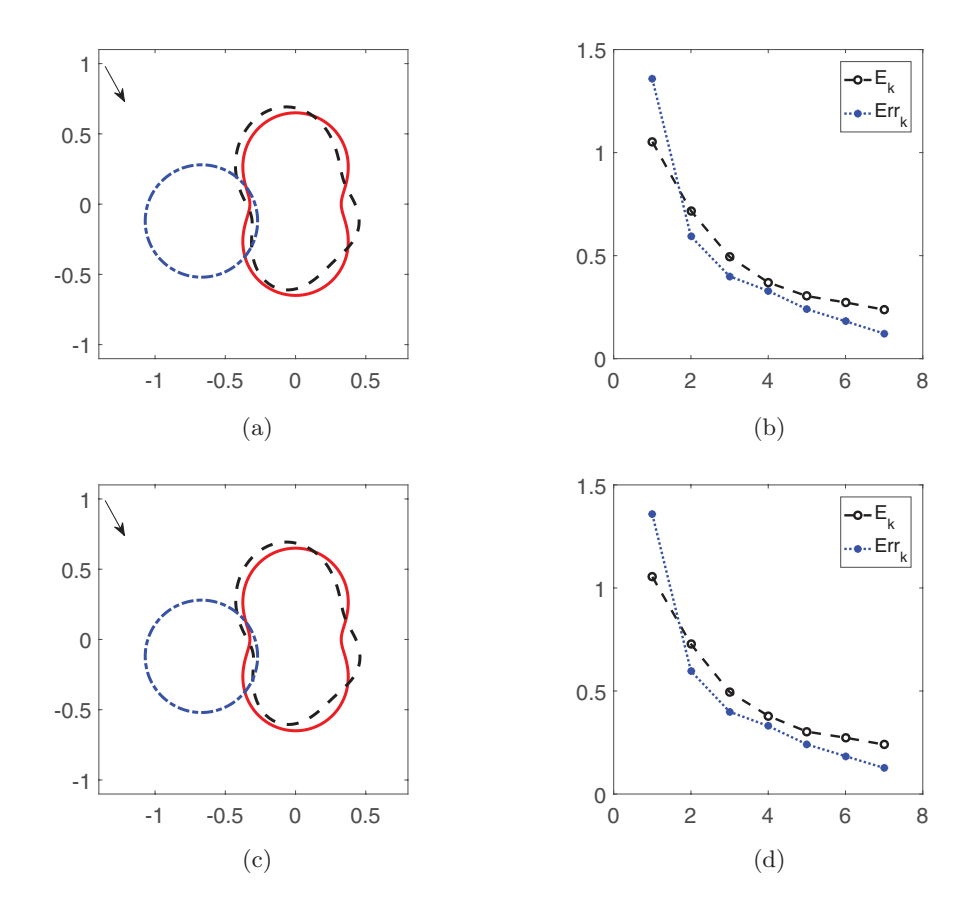


Figure 3. Reconstructions of a peanut-shaped obstacle with phased data at different levels of noise (see Example 1). The initial guess is given by $(c_1^{(0)}, c_2^{(0)}) = (-0.67, -0.12), r^{(0)} = 0.4$ and the incident angle $\theta = 13\pi/8$. (a) Reconstruction with 1% noise, $\epsilon = 0.25$. (b) Relative error with 1% noise. (c) Reconstruction with 5% noise, $\epsilon = 0.25$. (d) Relative error with 5% noise.

6.2.2. Discretization. Noting that the kernels of $S_{\kappa}^{\sigma,\varrho}$, $K_{\kappa}^{\sigma,\varrho}$ and $H_{\kappa}^{\sigma,\varrho}$ are weakly singular when $\sigma = \varrho$. With the help of quadrature rules (5.3)–(5.8), the full discretization of (6.11)–(6.13) can be handled the same as those described in section 5.

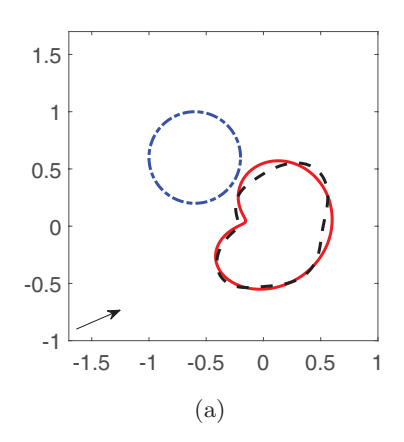
In addition, we introduce the following definition

$$\begin{split} &M_D(t,\varsigma;\varphi) := \gamma_{\kappa_a} \exp\left\{-\mathrm{i}\kappa_a \big(c_1 \cos t + c_2 \sin t + r(\varsigma) \cos(t-\varsigma)\big)\right\} \varphi(\varsigma), \\ &M_B(t,\varsigma;\varphi) := \gamma_{\kappa_a} \exp\left\{-\mathrm{i}\kappa_a \big(c_1 \cos t + c_2 \sin t + R \cos(t-\varsigma)\big)\right\} \varphi(\varsigma), \\ &\sum_{\sigma} S^{\infty}_{\kappa_a,\sigma} [\varphi_{3,\sigma} G_{\sigma};p_{\sigma}](\varsigma^{(\bar{n})}_i) = \frac{\pi}{n} \sum_{j=0}^{2n-1} \Big(M_D(\varsigma^{(\bar{n})}_i,\varsigma^{(n)}_j;\varphi_{3,D} G_D) + M_B(\varsigma^{(\bar{n})}_i,\varsigma^{(n)}_j;\varphi_{3,D} G_D)\Big). \end{split}$$

Then, we get the discretized linear system

$$\sum_{l=1}^{2} A_{l}^{c}(\varsigma_{i}^{(\bar{n})}) \Delta c_{l} + \sum_{m=0}^{M} \alpha_{m} A_{1,m}^{r}(\varsigma_{i}^{(\bar{n})}) + \sum_{m=1}^{M} \beta_{m} A_{2,m}^{r}(\varsigma_{i}^{(\bar{n})}) = \breve{w}(\varsigma_{i}^{(\bar{n})})$$
(6.18)

to determine the real coefficients Δc_1 , Δc_2 , α_m and β_m , where



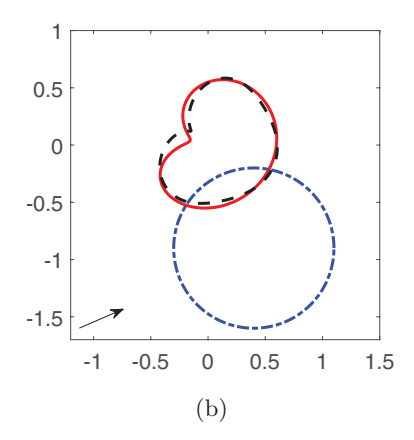
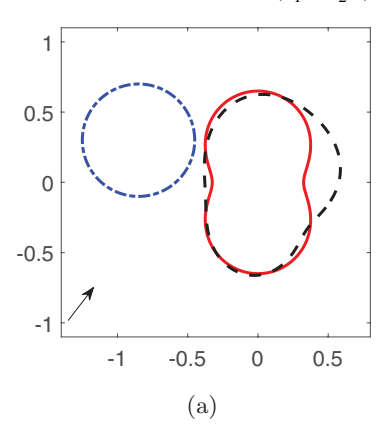


Figure 4. Reconstructions of an apple-shaped obstacle with different initial guesses, where 1% noise is added and the incident angle $\theta=\pi/6$. (a) $(c_1^{(0)},c_2^{(0)})=(-0.6,0.6)$, $r^{(0)}=0.4$, $\epsilon=0.2$; (b) $(c_1^{(0)},c_2^{(0)})=(0.4,-0.9)$, $r^{(0)}=0.7$, $\epsilon=0.15$ (see Example 1).



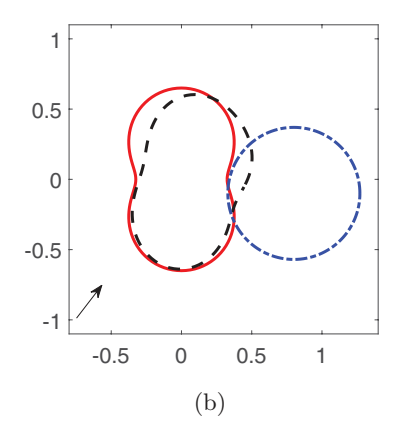


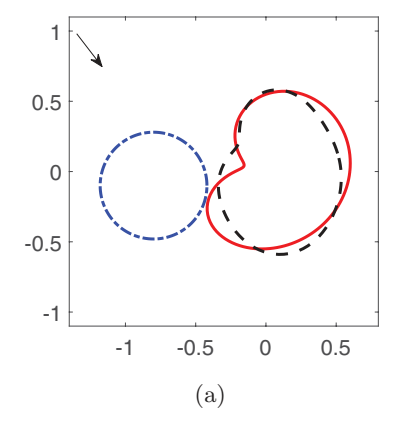
Figure 5. Reconstructions of a peanut-shaped obstacle with different initial guesses, where 1% noise is added and the incident angle $\theta=\pi/3$ (see Example 1). (a) $(c_1^{(0)},c_2^{(0)})=(-0.85,0.3), \ r^{(0)}=0.4, \ \epsilon=0.25;$ (b) $(c_1^{(0)},c_2^{(0)})=(0.8,-0.1), \ r^{(0)}=0.47, \ \epsilon=0.3.$

$$A_l^c(\varsigma_i^{(\bar{n})}) = 2\Re\left\{\frac{\pi}{n}\overline{\sum_{\sigma}S_{\kappa_a,\sigma}^{\infty}[\varphi_{3,\sigma}G_{\sigma};p_{\sigma}](\varsigma_i^{(\bar{n})})}\sum_{j=0}^{2n-1}L_l(\varsigma_i^{(\bar{n})},\varsigma_j^{(n)};\varphi_{3,D}G_D)\right\}$$

for l = 1, 2, and

$$A_{1,m}^r(\varsigma_i^{(\bar{n})}) = 2\Re\Big\{\frac{\pi}{n}\overline{\sum_{\sigma}}S_{\kappa_{\mathbf{a},\sigma}}^{\infty}[\varphi_{\mathbf{3},\sigma}G_{\sigma};p_{\sigma}](\varsigma_i^{(\bar{n})})\sum_{j=0}^{2n-1}L_{\mathbf{3},m}(\varsigma_i^{(\bar{n})},\varsigma_j^{(n)};\varphi_{\mathbf{3},D}G_{D})\Big\},$$

$$A_{2,m}^r(\varsigma_i^{(\bar{n})}) = 2\Re\Big\{\frac{\pi}{n}\overline{\sum_{\sigma}S_{\kappa_{\mathbf{a}},\sigma}^{\infty}[\varphi_{3,\sigma}G_{\sigma};p_{\sigma}](\varsigma_i^{(\bar{n})})}\sum_{j=0}^{2n-1}L_{4,m}(\varsigma_i^{(\bar{n})},\varsigma_j^{(n)};\varphi_{3,D}G_D)\Big\}.$$



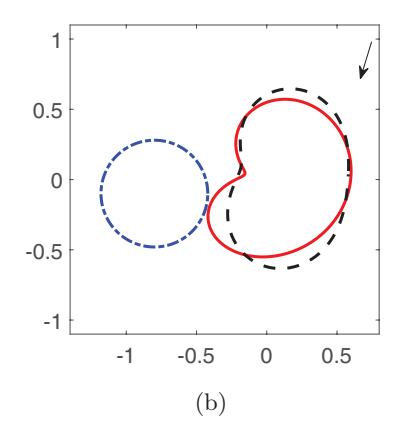
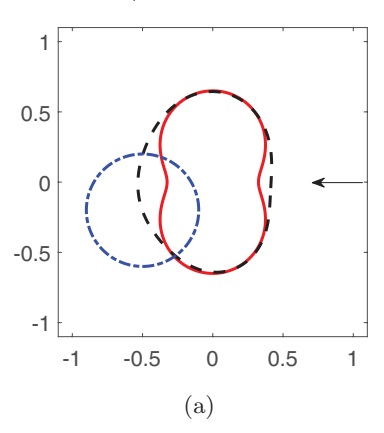


Figure 6. Reconstructions of an apple-shaped obstacle with different incident directions, where 1% noise is added and the initial guess is given by $(c_1^{(0)},c_2^{(0)})=(-0.8,-0.1)$, $r^{(0)}=0.38$ (see Example 1). (a) Incident angle $\theta=5\pi/3$, $\epsilon=0.2$; (b) incident angle $\theta=10\pi/7$, $\epsilon=0.2$.



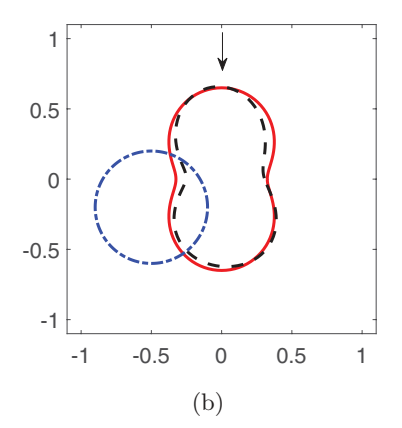


Figure 7. Reconstructions of a peanut-shaped obstacle with different incident directions, where 1% noise is added and the initial guess is given by $(c_1^{(0)}, c_2^{(0)}) = (-0.5, -0.2)$, $r^{(0)} = 0.4$ (see Example 1). (a) Incident angle $\theta = \pi, \epsilon = 0.2$; (b) incident angle $\theta = 3\pi/2$, $\epsilon = 0.2$.

Similarly, the overdetermined system (6.18) is also solved via the Tikhonov regularization with H^2 penalty term which is introduced in section 6.1.2.

7. Numerical experiments

In this section, we present some numerical examples to illustrate the feasibility of the iterative reconstruction methods. We use a single plane wave to illuminate the obstacle. The synthetic far-field data and phaseless far-field data are numerically generated by the Nyström-type method described in section 5. In order to avoid the inverse crime, the number of quadrature nodes used in the inverse solver (n=64) is chosen to be different from that of the direct solver (n=100). The noisy data $u_{\infty,\delta}$ and $|u_{\infty,\delta}|^2$ are generated in the following way

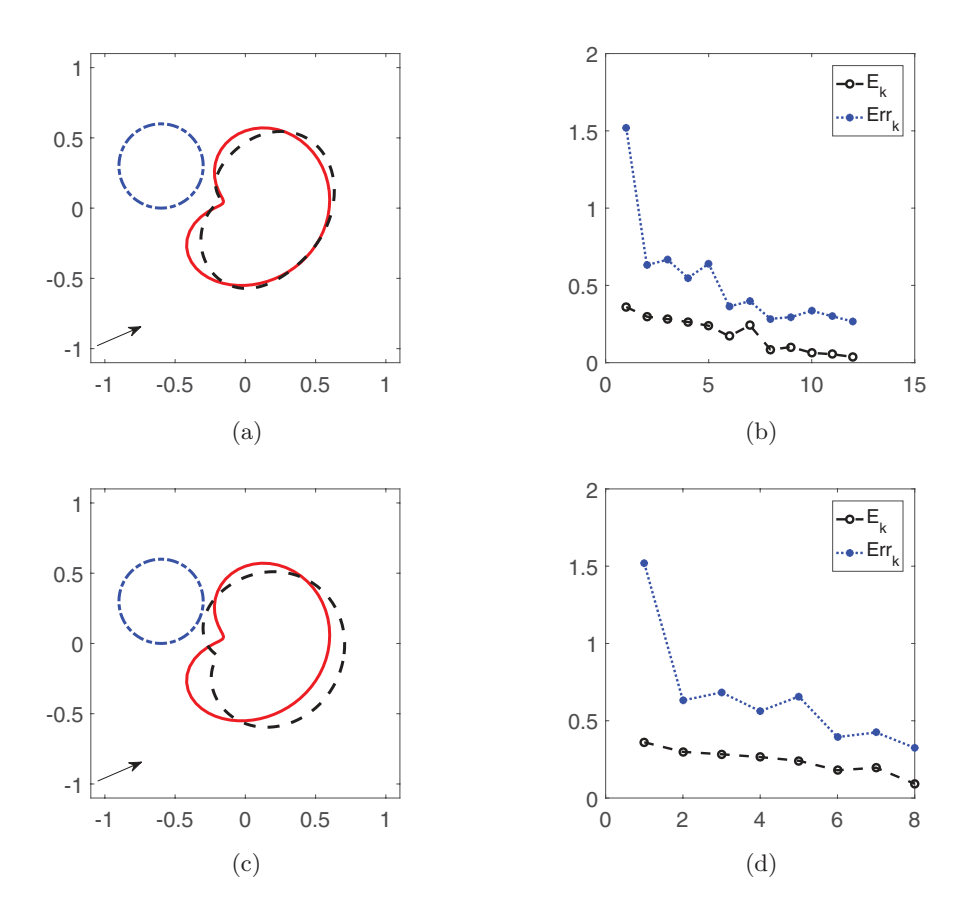


Figure 8. Reconstructions of an apple-shaped obstacle with different levels of noise by using phaseless data and a reference ball (see Example 2). The initial guess is given by $(c_1^{(0)},c_2^{(0)})=(-0.6,0.3), r^{(0)}=0.3$, the incident angle $\theta=\pi/6$, and the reference ball is $(b_1,b_2)=(6.2,0), R=0.74$. (a) Reconstruction with 1% noise, $\epsilon=0.05$. (b) Relative error with 1% noise. (c) Reconstruction with 5% noise, $\epsilon=0.1$. (d) Relative error with 5% noise.

$$u_{\infty,\delta} = u_{\infty}(1 + \delta \breve{\omega}), \quad |u_{\infty,\delta}|^2 = |u^{\infty}|^2 (1 + \delta \varpi),$$

where $\breve{\varpi} = \breve{\varpi}_1 + i\breve{\varpi}_2$, $\breve{\varpi}_1$, $\breve{\varpi}_2$ and ϖ are normally distributed random numbers ranging in [-1,1], $\delta > 0$ is the relative noise level. In addition, we denote the L^2 relative error between the reconstructed and exact boundaries by

$$Err_k := \frac{\|p_D^{(k)} - p_D\|_{L^2(\Omega)}}{\|p_D\|_{L^2(\Omega)}}.$$

In the iteration process, we obtain the update ξ from a scaled Newton step with the Tikhonov regularization and H^2 penalty term, i.e.

$$\xi = \rho (\lambda \widetilde{I} + \Re(\widetilde{B}^* \widetilde{B}))^{-1} \Re(\widetilde{B}^* \widetilde{w}),$$

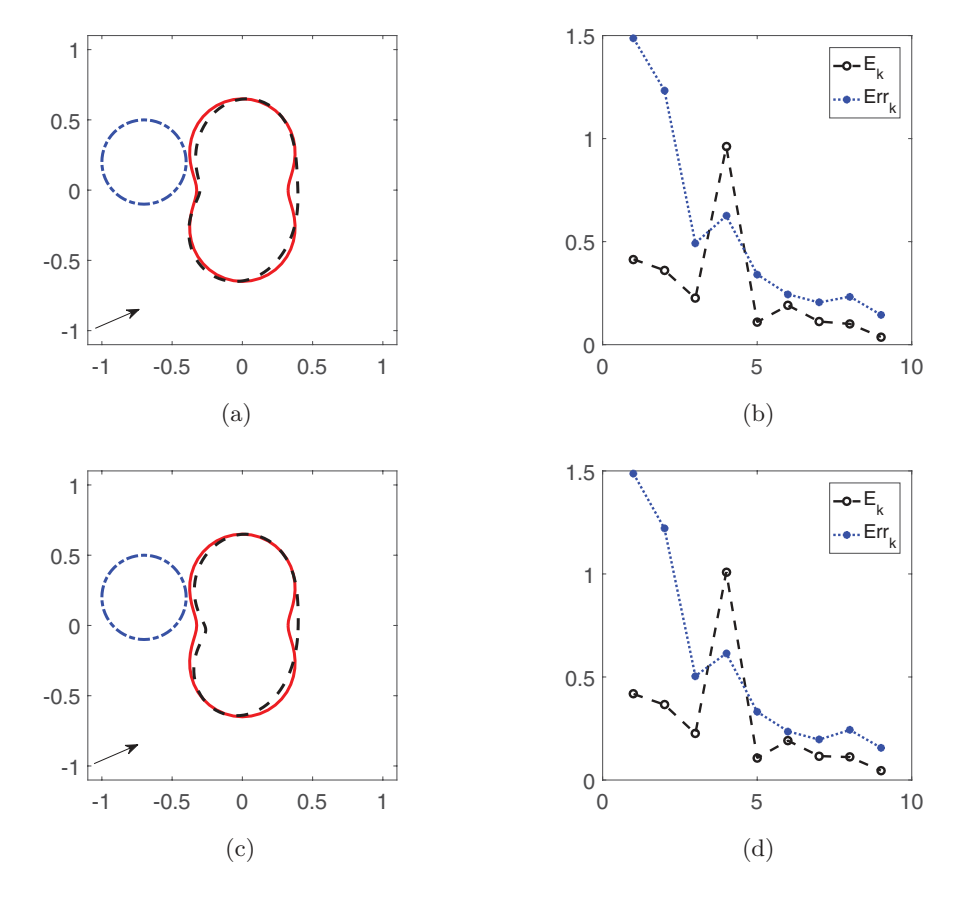
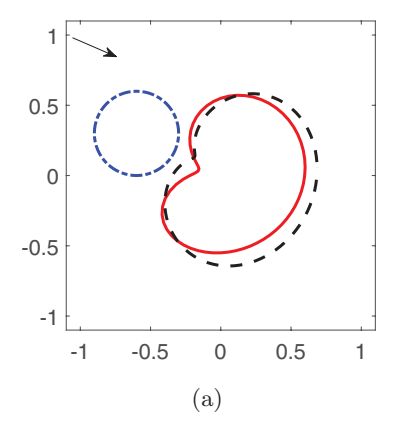


Figure 9. Reconstructions of a peanut-shaped obstacle with different levels of noise by using phaseless data and a reference ball (see Example 2). The initial guess is given by $(c_1^{(0)},c_2^{(0)})=(-0.7,0.2),r^{(0)}=0.3$, the incident angle $\theta=\pi/6$, and the reference ball is $(b_1,b_2)=(6.6,0),R=0.71$. (a) Reconstruction with 1% noise, $\epsilon=0.1$. (b) Relative error with 1% noise. (c) Reconstruction with 5% noise, $\epsilon=0.1$. (d) Relative error with 5% noise.

where the scaling factor $\rho \geqslant 0$ is fixed throughout the iterations. Analogously to [9], the regularization parameter λ in (6.7) is chosen as

$$\lambda_k := \left\| w_{\infty} - S_{\kappa_a}^{\infty} [\varphi_3 G; p^{(k)}] \right\|_{L^2}, \ k = 1, 2, \cdots.$$

In all of the following figures, the exact boundary curves are displayed in solid lines, the reconstructed boundary curves are shown in dashed lines —, and all the initial guesses are taken to be a circle which is indicated in the dash-dotted lines —. The incident directions are denoted by directed line segments with arrows. Throughout all the numerical examples, we take $\lambda=3.88, \mu=2.56$, the angular frequency $\omega=0.7\pi$, the densities $\rho_{\rm e}=2$ and $\rho_{\rm a}=1$, the wave number $\kappa_{\rm a}=2$, the scaling factor $\rho=0.9$, and the truncation M=6. We present the results for two commonly used examples: an apple-shaped obstacle and a peanut-shaped obstacle. The parametrization of the exact boundary curves for these two obstacles are given in table 1.



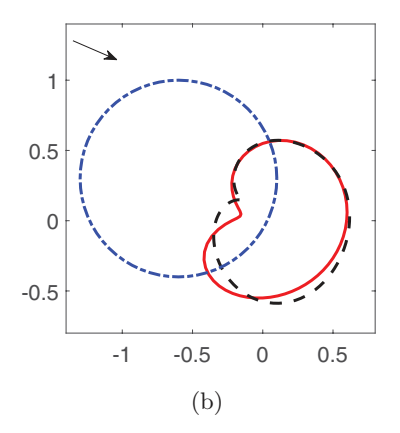
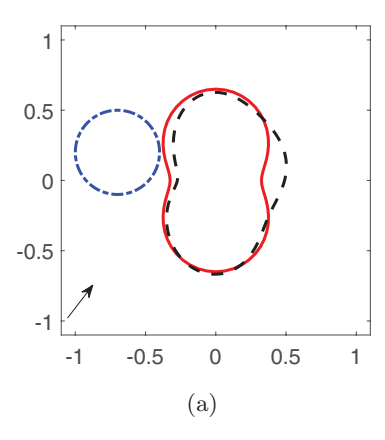


Figure 10. Reconstructions of an apple-shaped obstacle with different initial guesses, where 1% noise is added, the incident angle $\theta = 11\pi/6$, and the reference ball is $(b_1, b_2) = (6.2, 0), R = 0.65$ (see Example 2). (a) $(c_1^{(0)}, c_2^{(0)}) = (-0.6, 0.3), r^{(0)} = 0.3, \epsilon = 0.15$; (b) $(c_1^{(0)}, c_2^{(0)}) = (-0.6, 0.3), r^{(0)} = 0.7, \epsilon = 0.15$.



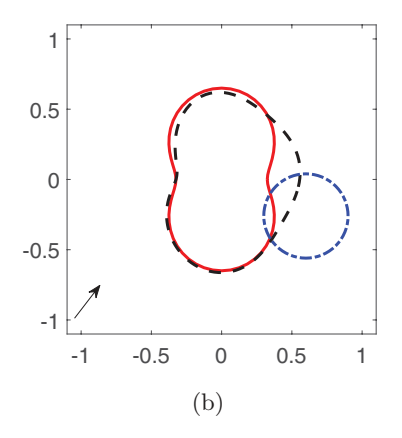
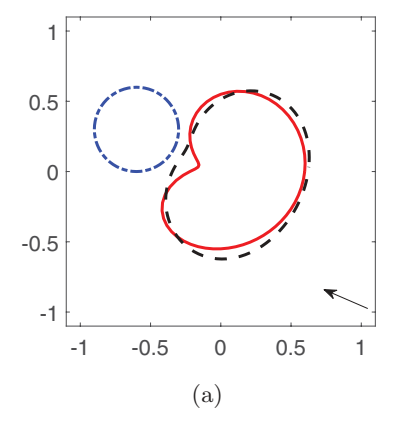


Figure 11. Reconstructions of a peanut-shaped obstacle with different initial guesses, where 1% noise is added, the incident angle $\theta = \pi/3$, and the reference ball is $(b_1, b_2) = (6.7, 0), R = 0.67$ (see Example 2). (a) $(c_1^{(0)}, c_2^{(0)}) = (-0.7, 0.2), r^{(0)} = 0.3, \epsilon = 0.1$; (b) $(c_1^{(0)}, c_2^{(0)}) = (0.6, -0.26), r^{(0)} = 0.3, \epsilon = 0.15$.

Example 1: The IAEIP with far-field data. We consider the inverse problem of reconstructing an elastic obstacle from far-field data by using algorithm I. The synthetic far-field data is numerically generated at 128 points, i.e. $\tilde{n}=64$. In figures 2 and 3, the reconstructions of an apple-shaped and a peanut-shaped obstacles with 1% and 5% noise are shown, respectively. Moreover, the relative L^2 error Err_k between the reconstructed and exact boundaries and the error E_k defined in (6.4) are also presented with respect to the number of iterations. As we can see from the figures, the trend of two error curves is basically the same for larger number of iteration. Therefore, the choice of the stopping criteria is reasonable. The reconstructions with different initial guesses for the two curves are given in figures 4 and 5, and the reconstructions with different directions of incident waves are presented in figures 6 and 7. As shown in these results, the location and shape of the obstacle could be simultaneously and satisfactorily reconstructed for a single incident plane wave.



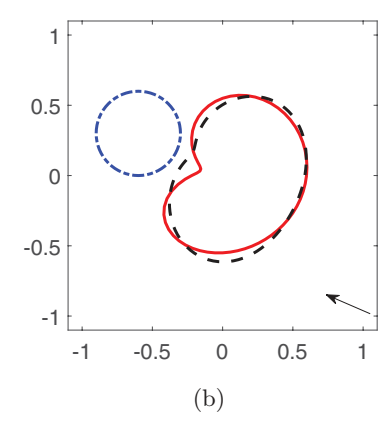
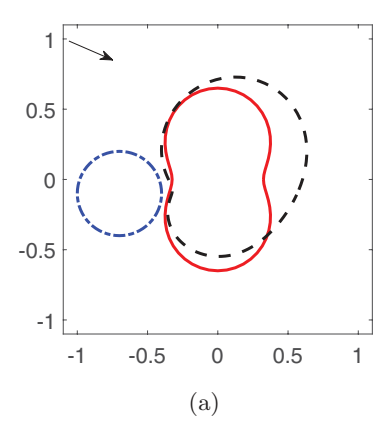


Figure 12. Reconstructions of an apple-shaped obstacle with different reference balls, where 1% noise is added, the incident angle $\theta = 5\pi/6$, and the initial guess is given by $(c_1^{(0)}, c_2^{(0)}) = (-0.6, 0.3), r^{(0)} = 0.3$ (see Example 2). (a) $(b_1, b_2) = (6, 0), R = 0.35, \epsilon = 0.2$; (b) $(b_1, b_2) = (-6, 0), R = 0.6, \epsilon = 0.15$.



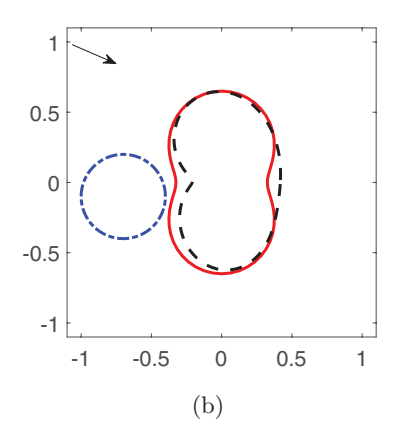


Figure 13. Reconstructions of a peanut-shaped obstacle with different reference balls, where 1% noise is added, the incident angle $\theta=11\pi/6$, and the initial guess is given by $(c_1^{(0)},c_2^{(0)})=(-0.7,-0.1),r^{(0)}=0.3$ (see Example 2). (a) $(b_1,b_2)=(-7.8,0),R=0.47,\epsilon=0.2$; (b) $(b_1,b_2)=(6.6,0),R=0.71,\epsilon=0.1$.

Example 2: The IAEIP with phaseless far-field data and a reference ball. By adding a reference ball to the inverse scattering system, we consider the inverse problem of reconstructing an elastic obstacle from phaseless far-field data based on algorithm II. The synthetic phaseless far-field data is numerically generated at 64 points, i.e. $\bar{n} = 32$. The reconstructions with 1% noise and 5% noise are shown in figures 8 and 9, respectively. Again, the relative L^2 error Err_k and the error E_k are presented in the figures. The reconstructions with different initial guesses for the two curves are given in figures 10 and 11. The reconstructions with different reference balls are shown in figures 12 and 13. From this example, we found that the translation invariance property of the phaseless far-field pattern can be broken down by introducing a reference ball. Based on this algorithm, both the location and shape of the obstacle can be satisfactorily reconstructed from the phaseless far-field data for a single incident plane wave.

8. Conclusions

In this paper, we have studied the 2D inverse acoustic scattering problem by an elastic obstacle with the phased and phaseless far-field data for a single incident plane wave. Based on the Helmholtz decomposition, the coupled acoustic-elastic wave equation is reformulated into a coupled boundary value problem of the Hemholtz equations, and the uniqueness of the solution for this boundary problem is proved. We investigate the jump relations for the second derivatives of single-layer potential and establish coupled boundary integral equations. We prove the well-posedness of the solution for the coupled boundary integral equations, and develop an efficient and accurate Nyström-type discretization to solve the coupled system. The method of nonlinear integral equations is developed for the inverse problem. In addition, we show that the phaseless far-field pattern is invariant under translation of the obstacle. To locate the obstacle, an elastic reference ball is introduced to the scattering system in order to break the translation invariance. We establish the uniqueness for the IAEIP with phaseless far-field pattern. A nonlinear integral equation method is proposed for the inverse problem. Numerical results show that the location and shape of the obstacle can be satisfactorily reconstructed. Future work includes the uniqueness for the phaseless inverse scattering with one incident plane wave and the extension of the method to the three-dimensional (3D) inverse scattering problem. For the 3D problem, since the Helmholtz decomposition leads to a system involving both the Helmholtz equation and the Maxwell equation, both numerical schemes and theoretical analysis become much more complicated. We are currently investigating the 3D problem and hope to report the progress elsewhere in the future.

Acknowledgments

The work of HD was partially supported by the NSFC Grants 11801213 and 11771180. The work of JL was partially supported by the Funds for Creative Research Groups of NSFC (No. 11621101), the Major Research Plan of NSFC (No. 91630309), NSFC Grant No. 11871427 and the Fundamental Research Funds for the Central Universities. The work of PL was supported in part by the NSF Grant DMS-1912704.

ORCID iDs

Jun Lai https://orcid.org/0000-0002-3044-5583 Peijun Li https://orcid.org/0000-0001-5119-6435

References

- [1] Ammari H, Chow Y T and Zou J 2016 Phased and phaseless domain reconstruction in inverse scattering problem via scattering coefficients SIAM J. Appl. Math. 76 1000–30
- [2] Bao G, Gao Y and Li P 2018 Time-domain analysis of an acoustic-elastic interaction problem Arch. Ration. Mech. Anal. 229 835–84
- [3] Bao G, Li P and Lv J 2013 Numerical solution of an inverse diffraction grating problem from phaseless data J. Opt. Soc. Am. A 30 293–9
- [4] Bao G and Zhang L 2016 Shape reconstruction of the multi-scale rough surface from multi-frequency phaseless data *Inverse Problems* 32 085002

- [5] Chen Z and Huang G 2016 A direct imaging method for electromagnetic scattering data without phase information SIAM J. Imaging Sci. 9 1273–97
- [6] Colton D and Kress R 1983 Integral Equation Methods in Scattering Theory (New York: Wiley)
- [7] Colton D and Kress R 2013 Inverse Acoustic and Electromagnetic Scattering Theory 3rd edn (New York: Springer)
- [8] Dong H, Lai J and Li P 2019 Inverse obstacle scattering for elastic waves with phased or phaseless far-field data SIAM J. Imaging Sci. 12 809–38
- [9] Dong H, Zhang D and Guo Y 2019 A reference ball based iterative algorithm for imaging acoustic obstacle from phaseless far-field data *Inverse Problems Imaging* 13 177–95
- [10] Elschner J, Hsiao G and Rathsfeld A 2008 An inverse problem for fluid-solid interaction *Inverse Problems Imaging* 2 83–119
- [11] Elschner J, Hsiao G and Rathsfeld A 2009 An optimization method in inverse acoustic scattering by an elastic obstacle *SIAM J. Appl. Math.* **70** 168–87
- [12] Gabor D 1948 A new microscopic principle Nature 161 777–8
- [13] Gao P, Dong H and Ma F 2018 Inverse scattering via nonlinear integral equations method for a sound-soft crack from phaseless data Appl. Math. 63 149–65
- [14] Hettlich F and Rundell W 1996 Iterative methods for the reconstruction of an inverse potential problem *Inverse Problems* 12 251–66
- [15] Hohage T 1997 Logarithmic convergence rates of the iteratively regularized Gauss–Newton method for an inverse potential and an inverse scattering problem *Inverse Problems* 13 1279–99
- [16] Hu G, Kirsch A and Yin T 2016 Factorization method in inverse interaction problems with bi-periodic interfaces between acoustic and elastic waves *Inverse Problems Imaging* 10 103–29
- [17] Ivanyshyn O 2007 Shape reconstruction of acoustic obstacles from the modulus of the far field pattern *Inverse Problems Imaging* 1 609–22
- [18] Ivanyshyn O and Johansson B T 2008 Boundary integral equations for acoustical inverse soundsoft scattering J. Inv. Ill-posed Problems 16 65–78
- [19] Ivanyshyn O and Kress R 2010 Identification of sound-soft 3D obstacles from phaseless data Inverse Problems Imaging 4 131–49
- [20] Ivanyshyn O, Kress R and Serranho P 2010 Huygens' principle and iterative methods in inverse obstacle scattering Adv. Comput. Math. 33 413–29
- [21] Ji X and Liu X 2019 Inverse elastic scattering problems with phaseless far field data *Inverse Problems* 35 114004
- [22] Ji X, Liu X and Zhang B 2019 Target reconstruction with a reference point scatterer using phaseless far field patterns SIAM J. Imaging Sci. 12 372–91
- [23] Ji X, Liu X and Zhang B 2019 Phaseless inverse source scattering problem: phase retrieval, uniqueness and sampling methods J. Comput. Phys. X 1 2590–0552
- [24] Jiang X and Li P 2017 An adaptive finite element PML method for the acoustic-elastic interaction in three dimensions *Comput. Phys.* 22 1486–507
- [25] Johansson T and Sleeman B D 2007 Reconstruction of an acoustically sound-soft obstacle from one incident field and the far-field pattern IMA J. Appl. Math. 72 96–112
- [26] Jones D S 1983 Low-frequency scattering by a body in lubricated contact Q. J. Mech. Appl. Math. 36 111–38
- [27] Karageorghis A, Johansson B T and Lesnic D 2012 The method of fundamental solutions for the identification of a sound-soft obstacle in inverse acoustic scattering Appl. Numer. Math. 62 1767–80
- [28] Kirsch A 1993 The domain derivative and two applications in inverse scattering theory *Inverse Problems* 9 81–96
- [29] Kirsch A and Ruiz A 2012 The factorization method for an inverse fluid-solid interaction scattering problem *Inverse Problems Imaging* 6 681–95
- [30] Klibanov M V, Nguyen D and Nguyen L 2019 A coefficient inverse problem with a single measurement of phaseless scattering data SIAM J. Appl. Math. 79 1–27
- [31] Kress R 2003 Newton's method for inverse obstacle scattering meets the method of least squares Inverse Problem 19 S91–104
- [32] Kress R 2014 Linear Integral Equations 3rd edn (New York: Springer)
- [33] Kress R and Rundell W 1997 Inverse obstacle scattering with modulus of the far field pattern as data *Inverse Problems Med. Imaging Nondestruct. Test.* 75–92

- [34] Lai J and Li P 2019 A framework for simulation of multiple elastic scattering in two-dimensions SIAM J. Sci. Comput. 41 A3276–99
- [35] Landau L D and Lifshitz E M 1986 Theory of Elasticity (Oxford: Pergamon)
- [36] Lee K M 2016 Shape reconstructions from phaseless data Eng. Anal. Bound. Elem. 71 174–8
- [37] Li J, Liu H and Wang Y 2017 Recovering an electromagnetic obstacle by a few phaseless backscattering measurements *Inverse Problems* 33 035011
- [38] Li J, Liu H and Zou J 2009 Strengthened linear sampling method with a reference ball SIAM J. Sci. Comput. 31 4013–40
- [39] Luke C J and Martin P A 1995 Fluid-solid interaction: acoustic scattering by a smooth elastic obstacle SIAM J. Appl. Math. 55 904–22
- [40] Monk P and Selgas V 2009 An inverse fluid-solid interaction problem *Inverse Problems Imaging* 3 173–98
- [41] Monk P and Selgas V 2011 Near field sampling type methods for the inverse fluid-solid interaction problem *Inverse Problems Imaging* 5 465–83
- [42] Potthast R 2001 On the convergence of a new Newton-type method in inverse scattering *Inverse Problems* 17 1419–34
- [43] Qu F, Yang J and Zhang B 2018 Recovering an elastic obstacle containing embedded objects by the acoustic far-field measurements *Inverse Problems* 34 015002
- [44] Shechtman Y, Eldar Y, Cohen O, Chapman H, Miao J and Segev M 2015 Phase retrieval with application to optical imaging IEEE Signal Process. Mag. 87–109
- [45] Sun F, Zhang D and Guo Y 2019 Uniqueness in phaseless inverse scattering problems with superposition of incident point sources *Inverse Problems* 35 105007
- [46] Taylor G 2003 The phase problem *Biol. Crystallogr.* **59** 1881–90
- [47] Xu X, Zhang B and Zhang H 2018 Uniqueness in inverse scattering problems with phaseless farfield data at a fixed frequency. II SIAM J. Appl. Math. 78 3024–39
- [48] Yin T, Hsiao G C and Xu L 2017 Boundary integral equation methods for the two dimensional fluid-solid interaction problem SIAM J. Numer. Anal. 55 2361–93
- [49] Yin T, Hu G, Xu L and Zhang B 2016 Near-field imaging of obstacles with the factorization method: fluid-solid interaction *Inverse Problems* 32 015003
- [50] Zhang D and Guo Y 2018 Uniqueness results on phaseless inverse scattering with a reference ball Inverse Problems 34 085002
- [51] Zhang D, Guo Y, Li J and Liu H 2018 Retrieval of acoustic sources from multi-frequency phaseless data *Inverse Problems* 34 094001
- [52] Zhang D, Sun F, Guo Y and Liu H 2019 Uniqueness in inverse acoustic scattering with phaseless near-field measurements *Inverse Problems and Imaging* (accepted)
- [53] Zhang D, Wang Y, Guo Y and Li J 2020 Uniqueness in inverse cavity scattering problems with phaseless near-field data *Inverse Problems* 36 025004
- [54] Zhang B and Zhang H 2017 Recovering scattering obstacles by multi-frequency phaseless far-field data J. Comput. Phys. 345 58–73
- [55] Zhang B and Zhang H 2018 Fast imaging of scattering obstacles from phaseless far-field measurements at a fixed frequency *Inverse Problems* 34 104005